CANADIAN THESES

THÈSES CANADIENNES

NOTICE

The quality of this microfiche is heavily dependent upon the quality of the original thesis submitted for microfilming. Every effort has been made to ensure the highest quality of reproduction possible.

If pages are missing, contact the university which granted the degree.

Some pages may have indistinct print especially if the original pages were typed with a poor typewriter ribbon or if the university sent us an inferior photocopy.

Previously copyrighted materials (journal articles, published tests, etc.) are not filmed.

Reproduction in full or in part of this film is governed by the Canadian Copyright Act, R.S.C. 1970, c. C-30.

AVIS

La qualité de cette microfiche dépend grandement de la qualité de la thèse soumise au microfilmage. Nous avons tout fait pour assurer une qualité supérieure de reproduction

S'il manque des pages, veuillez communiquer avec l'université qui a conféré le grade.

La qualité d'impression de certaines pages peut laisser à désirer, surtout si les pages originales ont été dactylographiées à l'aide d'un ruban usé ou si l'université nous a fait parvenir une photocopie de qualité inférieure

Les documents qui font déjà l'objet d'un droit d'auteur (articles de revue, examens publiés, etc.) ne sont pas microfilmés.

La reproduction, même partielle, de ce microfilm est soumise à la Loi canadienne sur le droit d'auteur, SRC 1970, c. C-30.

THIS DISSERTATION HAS BEEN MICROFILMED EXACTLY AS RECEIVED

LA THÈSE A ÉTÉ MICROFILMÉE TELLE QUE NOUS L'AVONS REÇUE

Epitaxial Gallium Arsenide

Giulio D'Asti

A Thesis

in

The Department

of

Electrical Engineering

Presented in Partial Fulfillment of the Requirements
for the Degree of Master of Engineering at
Concordia University
Montréal, Québec, Canada

March 1987

ISBN 0-315-35522-0

ABSTRACT

Epitaxial Gallium Arsenide

Giulio D'Asti

By the use of the Close Spaced Vapor Transport (CSVT), an epitaxial gallium arsenide (GaAs) thin film has been deposited on semi-insulating GaAs (SI GaAs). The epitaxial deposition has been confirmed by X-ray diffraction spectra and SEM observation of etch pit shapes and orientation (1).

The effects of hydrogen flux, source to substrate distances, transport temperature has been measured for SI GaAs deposited on SI GaAs using different spacer materials (semiconductor grade and high density grade graphite, boron nitrite, and fused silica (SiO_2)). These results have shown that the deposited films were n-type with a carrier concentration of 3.9×10^{16} to 1.15×10^{19} cm^{-3}, and with mobilities ranging from 151 to 3313 $cm^2 v^{-1} s^{-1}$ were obtained.

A thermodynamical model for the growth of GaAs, based

on the equilibrium constants of the reactions corresponding to the surfaces of the source and substrate temperatures, is summarized.

Using an equivalent thermal resistance circuit, a sample calculation is given on how to obtain the surface temperatures of the source and substrate.

The EL2 complex is described and analysed using the multilevel energy model. This complex is responsible for the existence of "undoped" semi-insulating GaAs.

From the different spacers used, a discussion on the probable cause for the measured high concentrations is given.

Semi-conducting as well as Semi-Insulating GaAs were successfully deposited on germanium substrates (Ge). GaAs/Ge is discussed as a future hetroepitaxial solar cell having a power conversion efficiency of 17 to 20%.

TABLE OF CONTENTS

LIST OF TABLES

LIST OF FIGURES

1. INTRODUCTION

20 years ago the technique of the Close Spaced Vapor Transport (CSVT) for thin film depositions was introduced by an RCA team (2). Since then, many semiconductors have been deposited using this technique (Ge, Si, CdS ,CdSe, CdTe, ZnSe, HgCdTe, $CuInS_2$, GaP, $GaAs_xP_{1-x}$, and GaAs) (1).

This research was aimed at investigating the effects of different sources and spacers in the CSVT reaction, to be able to control the carrier concentration of the deposited layers. This control of carrier concentrations would eventually permit the realization of an undoped Semi insulating Gallium Arsenide (SI GaAs) deposition. Such a deposition would be used in conjecture with germanium (Ge) for future integrated circuit manufacturing (3).

The second part of this investigation was aimed to successfully deposit Semi conducting (SC) and SI GaAs on germanium (Ge) for future solar cell fabrication using GaAs/Ge heteroepitaxial composition. The advantage of the CSVT lies in its simplicity and easiness for its industrial implementation (4). Thus, many variables were used to determine the reasons of high to low carrier concentrations of the deposited layers.

2. EXPERIMENTAL PROCEDURES

2.1 SI GaAs Wafers

The GaAs wafers were purchased from M/A Com Laser Diode Inc. All wafers used were of 0.5 mm in thickness, had an orientation of <100>, with a resistivity of $1x10^8$ ohm cm, and a dislocation density smaller than 10^5 per centimeter square. The wafers were polished on one side and 20 pieces of 1cm x 1cm were obtained once the wafer was cut. The 1cm square samples were used for sources and substrates.

2.2 Cleaning of SI GaAs Samples

The samples were cleaned in a refluxing acetone for a minimum period of 15 minutes. Both sources and substrates were etched at 80 degrees centigrade in a mixture of $H_2SO_4:H_2O_2:H_2O=(5:1:1)$ until a fine clean surface was obtained. The substrates were etched for a shorter amount of time. The samples were then rinsed with distilled water and dried with a nitrogen gun.

2.3 CSVT System

The CSVT system is shown in figure 1. The main part of the reaction chamber is made up of the graphite blocks held on a quartz tube, and the thermocouple entry tubes which are fitted in the blocks. The graphite blocks are $3x5x1$ cm^3. The entry holes are 0.7 cm and the quartz tubing for the thermocouples is 0.6 cm in diameter.

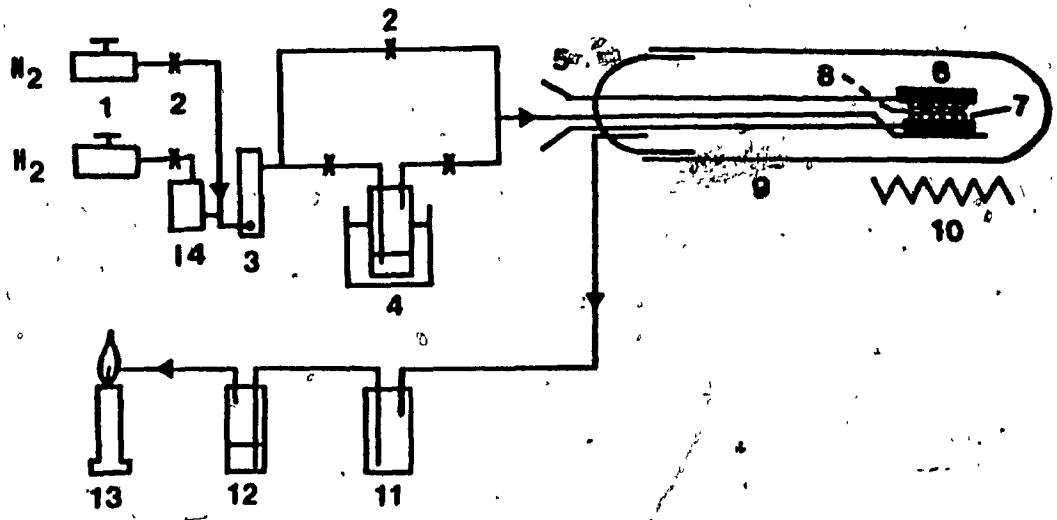

Fig. 1. Schematic representation of the CSVT deposition system: 1) N_2 and H_2 gas cylinders; 2) valves; 3) flow meters; 4) water saturator; 5) thermocouples; 6) graphite blocks; 7) GaAs source and substrate; 8) spacer; 9) quartz reactor tube; 10) 2000 W tungsten-halogen lamp; 11) trap; 12) glycerol bubbler; 13) burner; 14) hydrogen purifier.

The reaction tube is 37 cm long and 6 cm in diameter. It can be opened at one end. Teflon sleave is used to seal the opening. All internal and external parts are on the central right side of the graphite blocks. The quartz tubing has five little holes on its side. The system is heated by using a 2000 Watt tungsten halogen lamp on top of a gold plated reflector.

2.4 Epitaxial Conditions

The spacers used for this work were made of semiconductor grade purity graphite, high density graphite, boron nitride, and fused silica (SiO_2). The semiconductor grade graphite spacers had thicknesses ranging from 0.3 mm to 0.9 mm. The high density graphite spacer was 0.3 mm. The boron nitride spacers were 0.3 mm and 0.7 mm thick where the fused silica spacers had dimensions of 0.3 mm and 0.75 mm in thickness. All spacers had a hole of approximately 0.6 cm in diameter situated in the middle.

The graphite and boron nitride spacers were cleaned by degassing them in a nitrogen atmosphere at 750 degrees centigrade. The fused silica spacer was cleaned with the samples using the $H_2SO_4:H_2O_2:H_2O$ mixture. Once the samples and spacers were cleaned and installed in the system, the deposition procedures were started. First, nitrogen (N_2, Union Carbide 99.99% high purity) was passed through an oxisorb unit then to the system with a flow rate of 250 cc/min for 18 minutes. Dry hydrogen (H_2, Union

Carbide 99.999% ultra high purity) was then introduced in the system at 500 cc/min for 2 minutes. The hydrogen is passed through an oxisorb unit and a palladium diffusion hydrogen purifier (MBI HP-50), insuring less than 0.05 ppm of oxygen. After the 2 minutes, the hydrogen was passed through a water bubbler (water vapor transport reagent) for 10 minutes before the actual reaction. The water was maintained at 0 degrees celsius corresponding to a partial pressure of 609.14 Pa. At the 10 minute mark, the lamp was turned on, and the wet hydrogen was maintained for 10 to 12 minutes at 500 cc/min until the desired source temperature was stabilized. The hydrogen flow rate during the 20 minute deposition was between the range of 350 to 500 cc/min. The best temperature range was found to be 800 degrees celsius for all the investigated conditions. The measured temperature gradient between the source and substrate was kept at 50 degrees celsius plus or minus 10 degrees celsius. Once the reaction time was over, dry hydrogen was passed through the system with a flow rate of 500 cc/min for 10 minutes. After 10 minutes, the nitrogen was used to flush the system. The flushing lasted 10 minutes. The hydrogen was burned using a bunsen burner at the systems exhaust.

2.5 Transport Properties

The Hall effect measurements were performed by the use of the Van der Pauw method (5). The ohmic contacts were obtained by alloying the indium contacts in the GaAs at 500

degrees celsius in a hydrogen atmosphere for two minutes. The resistivity, carrier concentrations, mobilities, and Hall coefficients (for determining n or p type) were obtained. Most measures were made at room temperature (300 K). The thicknesses of the deposited layers were measured using a profilometer (Talysurf 4).

The equipment used for the Hall measurements consists of: A current source, a Keithley 225, the voltmeter was an HP 3455A digital voltmeter, and the magnet was from Walker Scientific. Figure 2 illustrates the above system.

2.6 Deposition Parameters as a Function of Epitaxial Growth

The parameters that have been varied during this work were a) the hydrogen flux, b) the thickness of the graphite spacer, c) the source and substrate temperature, d) the source (semi conductor), and e) the spacer material.

In following figures the results obtained for the different spacers (were applicable) and different conditions for each spacer are compared. The water used as a transport reagent was kept at 0 degrees celsius for all experimental work.

Figure 3 shows the variation of the growth rate (μm/min) versus the spacer thickness (mm). This variation was only performed with the semiconductor grade graphite blocks and spacers. The spacers ranged from 0.3 to 0.9 mm in thickness.

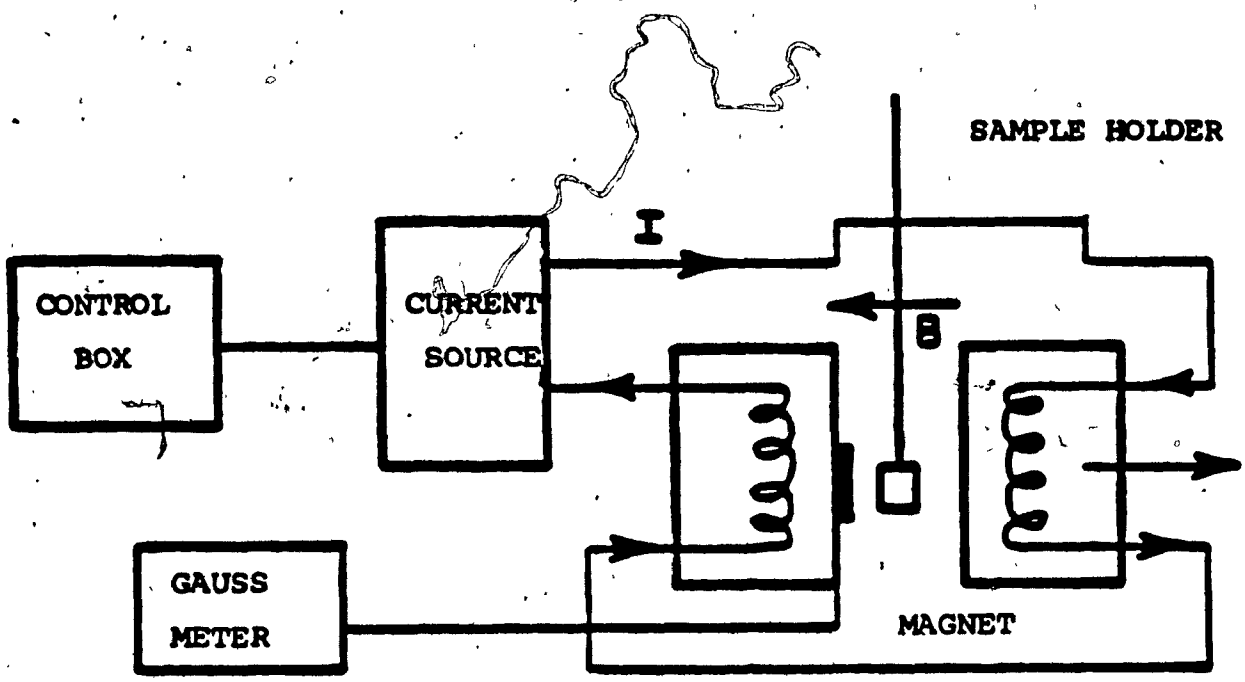

Fig. 2. Schematic representation of the characterizing apparatus.

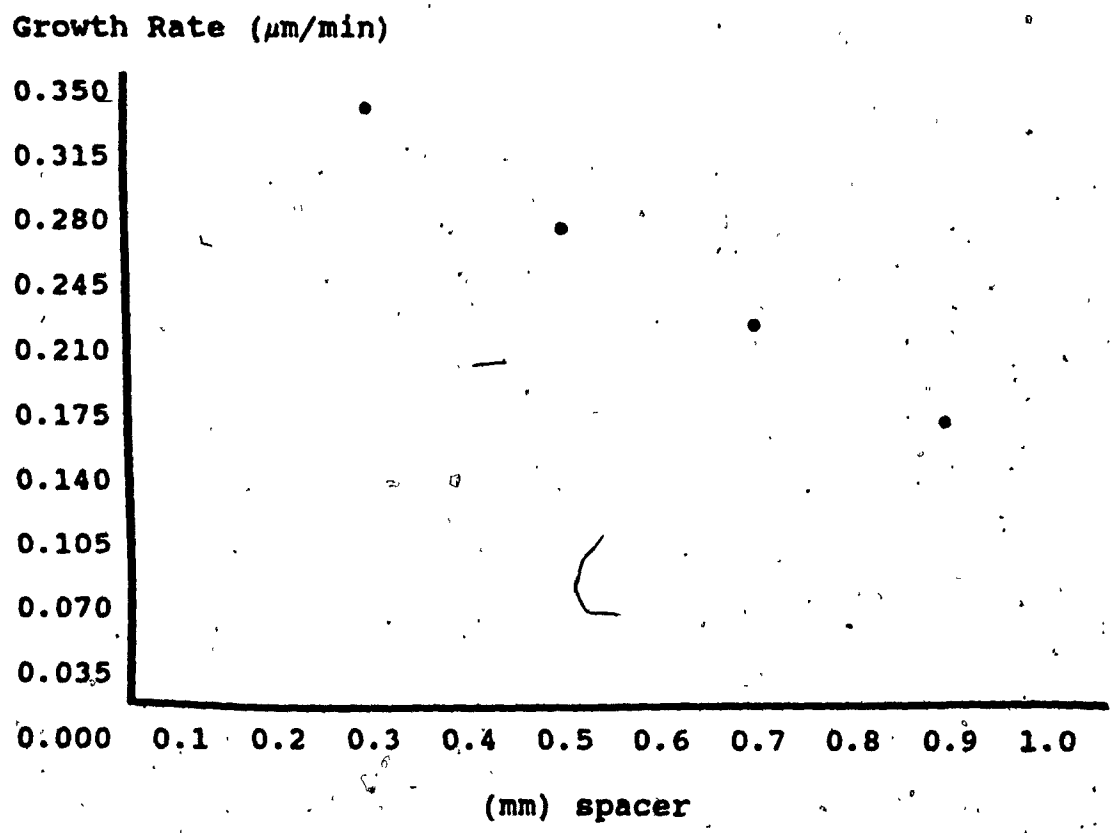

Fig. 3. Growth rate vs spacer thickness (semiconductor grade graphite blocks and spacer).

The growth rate in the above figure is defined as,

$$\text{Growth Rate} = d\ (\mu m)/t\ (min)$$

where d is the deposited film thickness and t is the deposition time. The deposition time used for figure 3 was 20 minutes. The temperature for this experiment was 1073 K for the source and 1023 K for the substrate. The hydrogen flow during deposition time was maintained at 500 cc/min.

Figure 4 shows the variation of the growth as a function of temperature. The semiconductor graphite spacer and blocks were used for the results of figure 4. The temperatures used were 1013, 1023, 1033, and 1073 K and the deposition time was also 20 minutes. From the above figures, it can be seen that as the temperature increases the growth rate also increases. At 1023 and 1033 K the growth rate is the same. This is due to the positioning of the samples on the graphite blocks. Some variation of temperature does exist along the blocks. Normally the samples are set as much as possible in the center of the blocks. However, if the samples are set much further away from the center the effective temperature can be altered. Because of the positioning, the actual temperature of the source sample was not 1033 K (as measured from the center of the graphite blocks) but 1023 K. This explains the similar results. The results presented in figure 4 were obtained by using the semiconductor graphite blocks and spacer of 0.8 mm.

Figure 5 shows the thickness dependence on deposition

time. As expected, the thickness increases with deposition time. Figure 6 illustrates the thickness versus the hydrogen flow. The difference between the samples measured was 0.4 μm. As previously shown (1), hydrogen flow does not affect the growth rate or thickness. The measurements from figures 5 and 6 were obtained using a 0.3 mm boron nitride spacer. The deposition temperature was 1023 K and the hydrogen flow rate for figure 5 was of 350 cc/min.

3. DISCUSSION

3.1 Thermodynamical Model for the Growth Rate Analysis

A solid which can react reversibly with a gas to form a volatile product, can be used for applications with the close spaced vapor transport method. For GaAs, the vapor transport reaction is expressed in the following form (6,7):

$$2GaAs(s)+H_2O(g) = Ga_2O(g)+As_2(g)+H_2(g) \quad /1/$$

At the deposition temperatures (1000 to 1100 K) , the presence of $As_4(g)$ molecules cannot be neglected. Therefore, the equilibrium between $As_2(g)$ and $As_4(g)$ has to be taken into consideration. This condition can be represented by the following expression (3):

$$\log (P_{As4}/P_{As2}) = -1980/T + 1.54 \quad /2/$$

Equation /1/ is then modified, and the second path for the transport of GaAs is obtained as (1):

$$2GaAs(s)+H_2O(g) = Ga_2O(g)+1/2As_4(g)+H_2(g) \quad /2a/$$

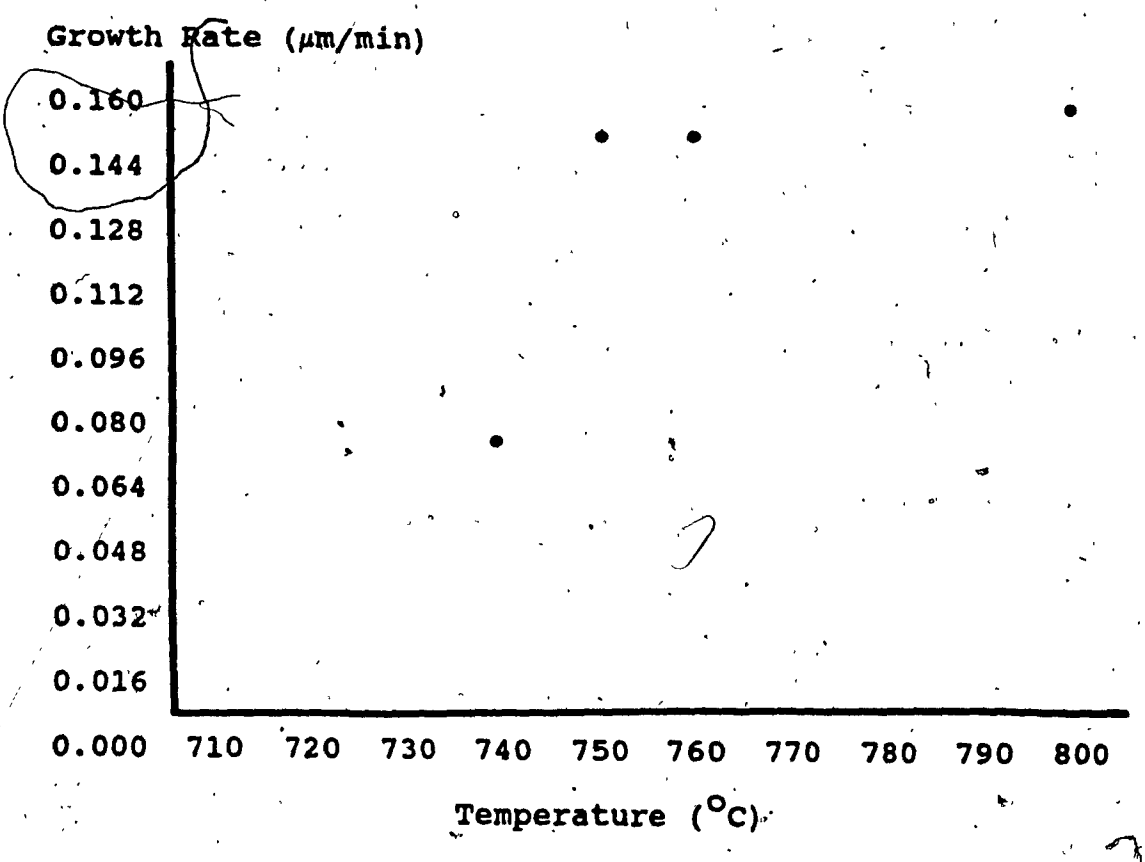

Fig. 4. Growth rate vs temperature (semiconductor grade graphite blocks and spacer).

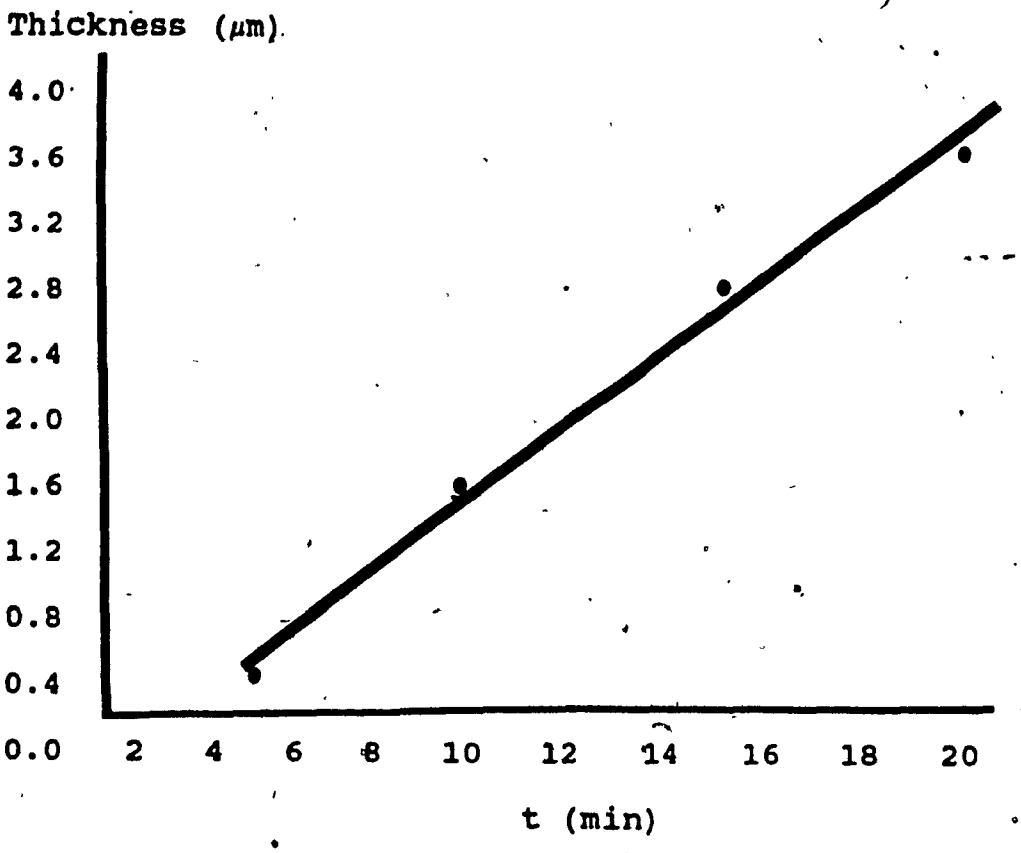

Fig. 5. Thickness vs time (semiconductor grade graphite blocks with boron nitrite spacer at T = 1023 K).

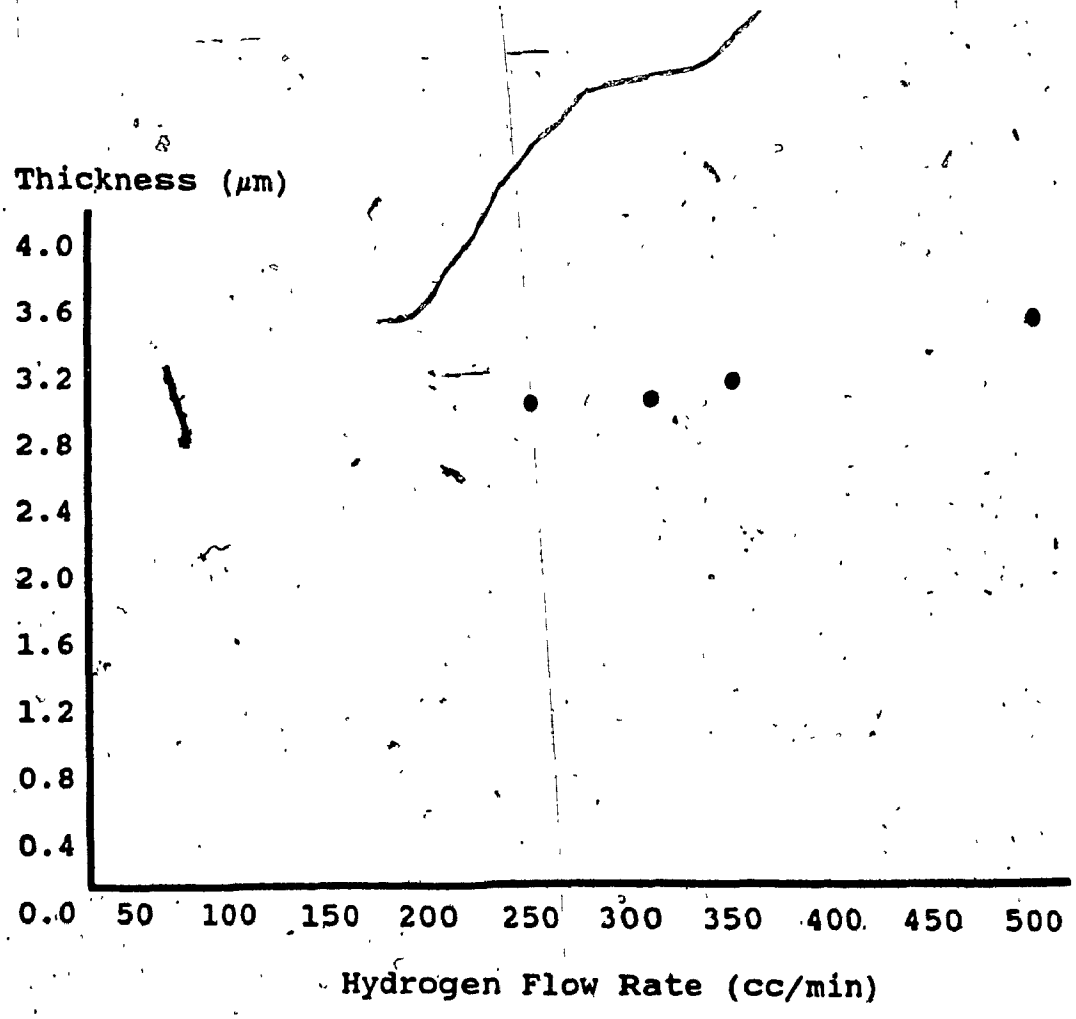

Fig. 6. Thickness vs hydrogen flow rate (semiconductor grade graphite blocks with 0.3 mm boron nitrite spacer at T = 1023 K).

These two equilibria, for the transport of GaAs on GaAs, are established at two temperatures (3):

(i) the GaAs source temperature T_1 and

(ii) the GaAs substrate temperature T_2, which correspond to the respective surfaces separated by the spacer.

The following assumptions are used in order to calculate the growth rate related to the displacement of the thermodynamical equilibrium constants of equation /1/, including the parallel expression due to equation /2/:

(i) the volatile components were constant at the source and substrate surface temperatures (T_1 and T_2) during the transport of GaAs. Therefore, the concentrations of Ga_2O and As_2 or As_4 can be determined by the equilibrium constants of the reactions.

(ii) a concentration gradient of the volatile products is established between the source and substrate, due to the displacement of the equilibirum constant T_1 and T_2. This concentration gradient depends on their respective concentrations at the source and substrate and their spatial separation. Therefore, the driving force of the reaction is the concentration gradient induced by the thermodynamic equilibrium displacement. This occurrence is due to the average mean free path of the gases of the reactive species in the temperature range of the reaction at atmospheric pressure (0.5 mm) which is commensurable with the separation of the two reactive surfaces (0.3 mm) (3).

For the reaction given by equation /1/, the thermodynamic equilibrium constants, K, at T_1 and T_2 can be written as (3):

$K(T_1)r = p^2(T_1) = r \exp(-\Delta G^o(T_1)/R(T_1))$, /3/ and

$k(T_2)r = p^2(T_2) = r \exp(-\Delta G^o(T_2)/R(T_2))$ /4/

where $p(Ga_2) = p(As_2) = p$, (p is the partial pressure of the volatile components), $r = p(H_2O)/p(H_2)$ is constant, ΔG^o is the standard free energy of reaction /1/ and R is the universal gas constant.

By considering the steady state fluxes of the volatile components, the growth rate of GaAs by CSVT can be determined. As an example, the case of Ga_2O:

$$J(Ga_2O) = D(1/d)p(T_1)/R(T_1) - p(T_2)/R(T_2), \quad /5/$$

where d is the separation between the source and substrate, D is the diffusion coefficient of Ga_2O in hydrogen at a mean temperature, T, between T_1 and T_2, and the term on the right hand side represents the concentration gradient of the volatile components.

The diffusion coefficient for a gas molecule x, in another gas y, is given by (1):

$$D_{xy} = (3RT/8(P_x+P_y)((\sigma_x+\sigma_y)/2)^2 \cdot ((RT/2\pi)(m_x+m_y)/(m_x \cdot m_y))^{1/2} \quad /5a/$$

where y is H_2, σ is the molecular diameter, m is the molar mass, and T is the average temperature between T_1 and T_2.

From equation /5a/, the diffusion coefficients of the volatile species can be determined, and the computed values

at 1000 K in hydrogen are :1.6, 4.1, and 1.6 cm squared/sec for Ga_2O, As_2 and As_4, respectively (1). If substitution is made from equations /3/ and /4/ to equation /5/, (taking into account that there are two Ga atoms transported by one molecule of Ga_2O), one obtains for the steady state Ga flux, J(Ga) (3):

$$J_{Ga} = 2 D_{Ga_2O,H_2} \times 1/\delta((K(T_1)r)^{1/2}/RT_1 - (K(T_2)r)^{1/2}/RT_2)) \quad /6/$$

Expressions for the other volatile components can be obtained similarly.

From equation /2/, the fraction of arsenic present as As_4, f, and as As_2, 1-f, can be determined. According to the assumptions of the model used in this investigation, both of the reactions represented by equations /1/ and /2/ reach their corresponding equilibrium independently. Consequently, the total flux of Ga transport J_{Ga}^t, and of As, J_{As}^t, can be expressed as

$$J_{Ga}^t = fJ'_{Ga} + (1-f)J_{Ga} \quad /7/ \text{ and}$$

$$J_{As}^t = fJ'_{As} + /(1-f)J_{As} \quad /8/.$$

where the reaction related to the As_4 species, according to equation /2/, is referred to by the primed fluxes.

As seen from the results, the diffusion coefficients of Ga_2O and As_4 are the same, and since both of these are less than that of As_2, the growth rate of GaAs characterized by the reaction given in equation /1/ can be obtained from the total steady state Ga flux given in equation /7/.

3.2 Temperature Corrections

The normal temperature values of T_1 and T_2 measured in the graphite blocks were corrected to obtain temperatures T_{1c} and T_{2c} measured on the surface of the samples. These new temperatures are necessary for the growth rate calculations of GaAs, since both reversible reactions occur at the surfaces of the source and substrate samples where the equilibrium in the CSVT is found. To calculate the new temperature differences between samples (source and substrate), a thermal equivalent circuit is considered for the CSVT system. Figure 7 shows the equivalent thermal circuit (1).

Before calculating the new temperatures, four factors must be considered. These factors are:

(i) the convection forces due to the flux of wet hydrogen in the reactor; (ii) the natural convection of the gases in the micro reaction chamber, where the hottest gas near the source is rising up to the substrate and the coldest gas near the substrate is descending towards the source; (iii) the existing radiation between the two graphite blocks heating the source and the substrate (GaAs is transparent to IR radiation up to about 1.5 eV); and (iv) the related conduction to the graphite under the source; the GaAs source, the numerous spacers, hydrogen in the micro reaction chamber, the GaAs substrate, and the graphite blocks heating the substrate.

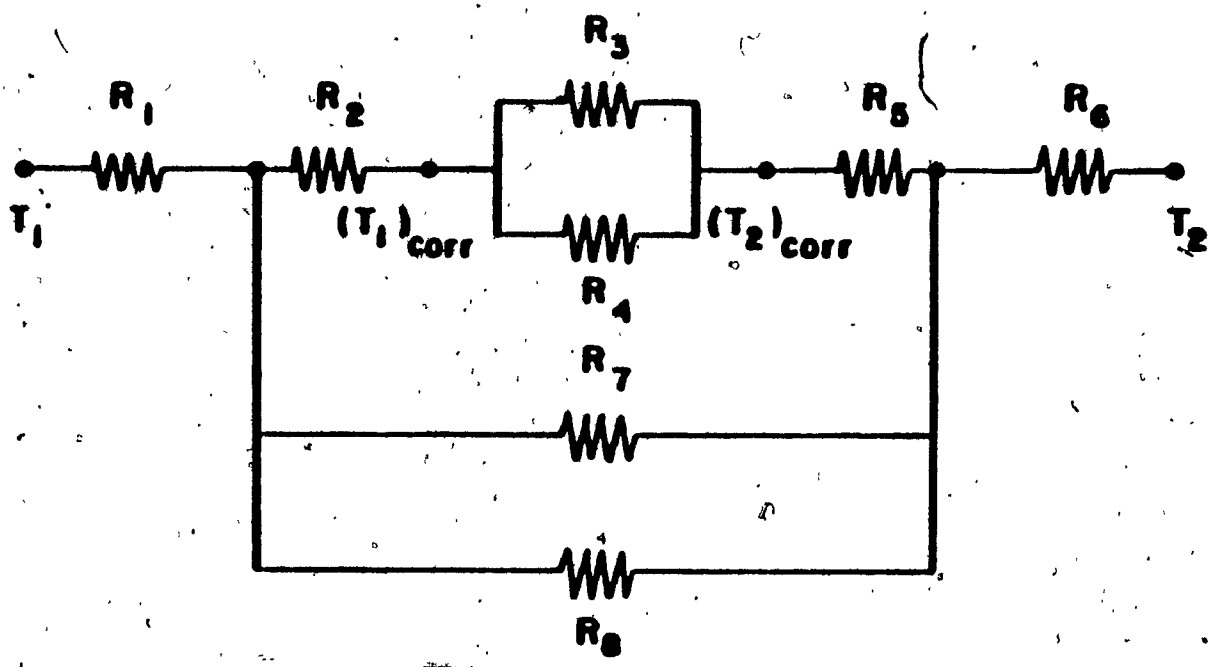

Fig. 7. Thermal equivalent circuit for the system graphite-source-spacer-substrate-graphite used in the CSVT epitaxy of GaAs.

It has been shown that the first and second factors could be disregarded in the CSVT reaction (1). Therefore, only the third and fourth factors are considered to obtain the corrected temperatures.

The thermal circuit shown in figure 7 is the equivalent to the system graphite-source-spacer-substrate-graphite. The thermal resistances are defined as follows:

R1 = bottom graphite sheet ($3x5x0.15\ cm^3$; where 0.15 cm is the graphite thickness between the thermocouple and the top of the block)

R2 = GaAs source ($1x1x0.06\ cm^3$)

R3 = spacer (fused silica, graphite, etc)

R4 = conduction by H2 in the micro reaction chamber

R5 = GaAs substrate ($1x1x0.06\ cm^3$)

R6 = top graphite sheet ($3x5x0.15\ cm^3$)

R7 = radiation between the two graphite blocks

R8 = conduction by H2 between the two graphite blocks.

Using the information given in Table I, the real temperature difference can be calculated.

$$Q = \sigma(T_1^4 - T_2^4)(1/\epsilon_1+1/\epsilon_2 - 1) \quad (Wcm^{-2})$$

represents the quantity of heat exchanged by radiation between two parallel plates. σ is the Boltzman constant ($5.67x10\text{-}12\ WK^{-4}cm^{-2}$) and ϵ is the emissivity of the graphite plates. The heat quantity exchanged by conduction perpendicular to the graphite block surfaces, is given by;

$$Q = \lambda A \Delta T/\Delta x\ (Wcm^{-2})$$

where λ is the thermal conductivity coefficient (W/cmK) and

A is the sample area.

Thus, from the above expressions the thermal resistance can be calculated as

$$R = \Delta T/Q = \Delta\chi/\lambda A \ (kW^{-1}cm^2) \quad (1).$$

TABLE I Materials conductivity coefficient and emissivity.

Material	$\lambda(Wcm^{-1}K^{-1})$	ϵ
Graphite	0.6 (1)	0.81 (9)
H_2	$4.28x10^{-3}$ (10)	
GaAs	0.15 (1)	
Fused Silica	$2.87x10^{-2}$ (8)	

All the above are for T = 998 ± 25 K.

The eight thermal resistances can now be calculated for T = 998 ± 25K.

$R1 = \Delta\chi/\lambda A = 3x5x0.15/0.6(3x5) = 0.167 \ (kW^{-1}cm^2)$

$R2 = 1x1x0.06/0.15x1 = 0.4$

$R3 = 1.2x0.03/2.87x10^{-2}x1.2 = 1.05$

$R4 = 2\pi x0.325x0.03/4.23x10^{-3}x2\pi x0.325 = 7.009$

$R5 = R2 = 0.4$

$R6 = R1 = 0.167$

$R7 = \Delta T/Q = 50/1.66 = 30.12$

$R8 = 3x5x(0.06x2 + 0.03)/4.28x10^{-3}x3x5 = 35.05$

$R34 = 0.913$, $R78 = 16.2$, $R2345 = 1.713$, $R2$ to $R8 = 1.633$, finally R equivalent = 1.967 ($kW^{-1}cm^2$).

To determine ΔT_1 and ΔT_2 corrected, the corresponding temperatures to each grouping of thermal resistances must be obtained. Therefore, knowing ΔT is 50 K the following branch temperatures can be calculated;

50 x R1/(R equivalent) = 4.245

50 x R2 to R8/(R equivalent) = 41.51

50 x R6/(R equivalent) = 4.245

Knowing the temperature of wanted branches (41.51 K), the corrected temperatures can be obtained;

41.51 x R2/(R2345) = 9.693

41.51 x R34/(R2345) = 32.12

41.51 x R5/(R2345) = 9.693

Therefore, ΔT_1 corrected is 9.693 - 32.12 = -12.43 K and ΔT_2 corrected is 32.12 - 9.693 = 12.43 K. From the results, it is simple to see that $T_{1c} = T_1 - 12.42$ K and $T_{2c} = T_2 + 12.43$ K. The ΔT corrected is of 50 - 12.43x2 = 25.14 K. The above calculation was done for a 0.3 mm fused silica spacer. The same procedure can be used to calculate the corrected temperatures for the other spacers.

In figure 8, (growth rate vs 1/T) (1) it is to be noted that the slope of the straight line is not associated with the activation energy corresponding to the surface reaction rate control.

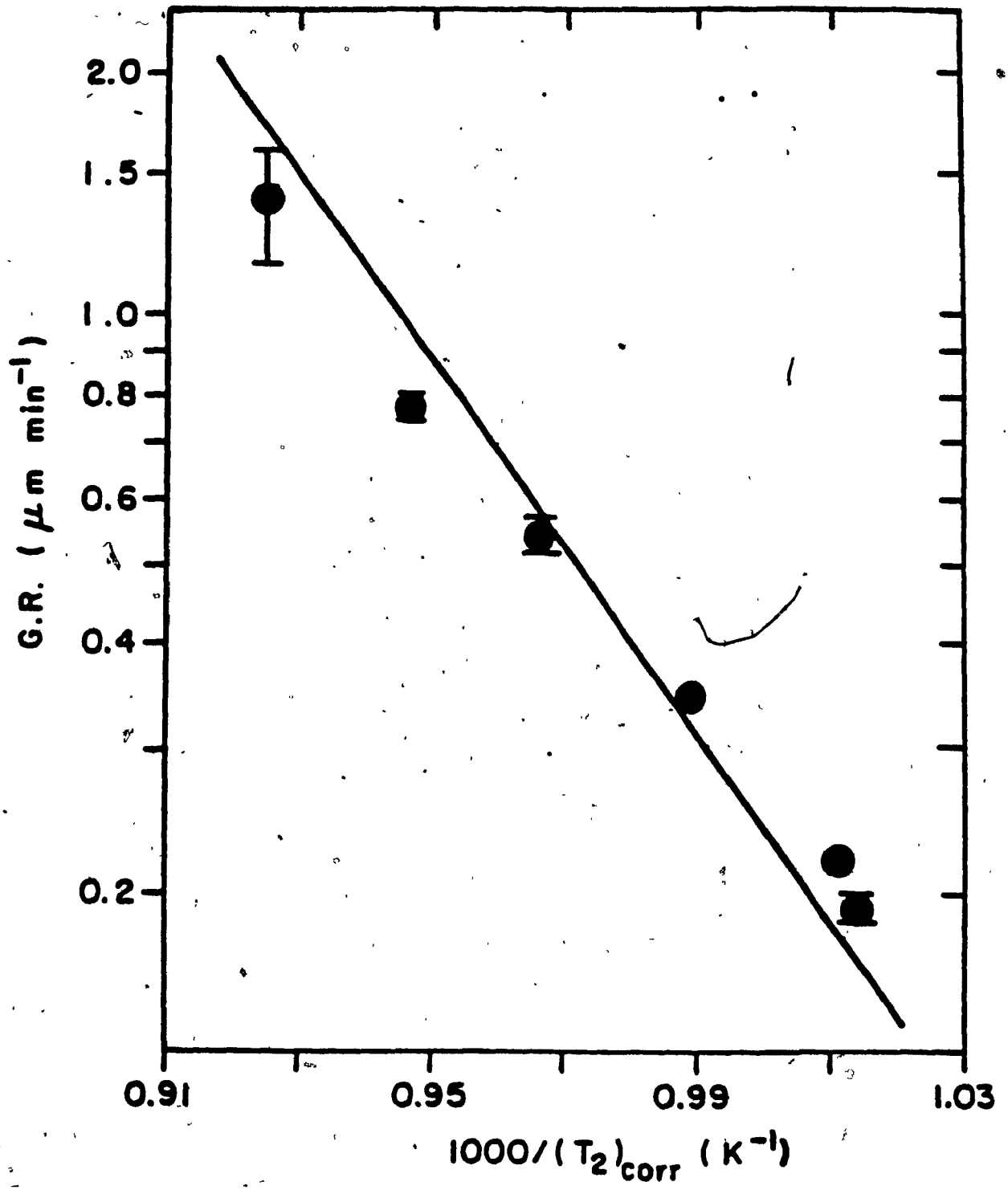

Fig. 8. Growth rate vs the inverse temperature, T_{2c}, at the surface of the GaAs substrate. The curve is calculated from the model.

From the model discussed in this investigation, the exponential dependence of the growth rate upon 1/T reflects the equilibrium constant displacement, equations /3/ and /4/, of the reaction described in equation /1/ as a function of temperature. Since the reversible reaction given in equation /1/ is always at equilibrium at the source and substrate surfaces, the classical reaction kinetics do not control the growth rate of the CSVT system. Therefore, the only two controlling factors of the deposition rate and film thickness uniformity for the epitaxial GaAs layers are the two temperatures (3).

3.3 Electrical Transport Properties and Measurements

The characteristics of the epitaxial layers (Hall coefficient, mobility and resistivity) were measured at room and liquid nitrogen temperatures. The Van der Pauw technique was used to perform the measurements. The technique was employed according to the ASTM specifications (27). The ohmic contacts were obtained by using indium alloyed at 500 degrees celsius in a hydrogen atmosphere (28). The Hall mobilities measured at room temperature were between 151 to 3313 $cm^2v^{-1}s^{-1}$ for the various spacers and graphite blocks used. In the case of the free electron concentrations measurements of $3.90x10^{16}$ to $1.15x10^{19}$ cm^{-3} were obtained.

Table II shows the difference in the measured results corresponding to the different conditions, the used spacers

and graphite blocks, for the depositions. The first epitaxial layers were grown using a fused silica spacer (SiO_2) and graphite blocks of semiconductor grade. The blocks were 3x5x1 cm^3. The fused silica spacer was then replaced by a graphite spacer of semiconductor grade. The spacer was 0.8 mm in thickness. This spacer was later reduced to 0.3 mm. The boron nitride spacers were then used replacing the graphite spacer. The boron nitride spacers had thickness' of 0.3 mm and 0.7 mm. When the boron nitride spacers were replaced by a high density graphite spacer of 0.3 mm, the blocks were also replaced by high density graphite blocks. The final change was made when the high density graphite spacer was replaced by a 0.3 mm fused silica spacer. The combination of the high density graphite blocks, and the fused silica spacer gave the best results. This combination gave the lowest free charge carrier concentration and the highest mobility.

The semiconductor grade graphite being more porous than the high density graphite was prone to more outside contamination. The absorption rate was greater. When the high density graphite was used, the free carrier concentration dropped by a factor of ten. This clearly shows that the graphite used (blocks and spacers) can alter the results. The fused silica spacer being even less porous than the high density graphite spacer reduced the concentration by a factor of two. The goal of this investigation was to reduce the free carrier concentration

to a minimum ($1x10^{14}$ to $1x10^{15}$ cm^{-3}) and increase the mobility to a maximum (5000 to 8000 $cm^2v^{-1}s^{-1}$). Hence, obtain a SI GaAs epitaxial layer.

TABLE II Experimental Results Under Different Conditions

---

1) Semiconductor Graphite Blocks (3x5x1 cm^3)

a) Fused silica (SiO_2) spacer (0.75 mm, 1073 K)

$n(cm^{-3})$	$\mu(cm^2v^{-1}s^{-1})$
$4.3x10^{17}$ to $1.05x10^{18}$	3012 to 2436

b) Semiconductor Graphite Spacers

(0.8 mm, 1013 K to 1033 K)

$n(cm^{-3})$	$\mu(cm^2v^{-1}s^{-1})$
$7.24x10^{17}$ to $1.15x10^{19}$	2105 to 151

(0.3 mm, 1073 K)

$5.46x10^{17}$ to $1.84x10^{18}$	2016 to 1205

c) Boron nitride Spacer (0.7 mm, 1073 K)

(0.7 mm, 1073 K)

$n(cm^{-3})$	$\mu(cm^2v^{-1}s^{-1})$
$4.89x10^{18}$	524

(0.3 mm, 1023 K)

$3.39x10^{17}$ to $1.91x10^{18}$	1982 to 1180

2) High Density Graphite Blocks (3x5x1 cm^3)

a) High Density Graphite Spacer (0.3 mm, 1023 K)

$n(cm^{-3})$	$\mu(cm^2v^{-1}s^{-1})$
$7.66x10^{16}$ to $1.61x10^{17}$	3125 to 1873

b) Fused silica (SiO_2) spacer (0.3 mm, 1023 K)

$n(cm^{-3})$	$\mu(cm^2v^{-1}s^{-1})$
$3.9x10^{16}$ to $4.64x10^{16}$	3313 to 1948

Figure 9 illustrates the mobility variation versus the charge concentration for the 0.75 mm fused silica spacer using the semiconductor graphite blocks. The deposition temperature was 1073 K and the hydrogen flow rate was 500 cc/min. The obtained result is what is expected. Only one measurement was not in the normal bound. As stated earlier, the most common error in the CSVT method, which can occur, is the placement of the samples on the graphite blocks. This misplacement caused a decrease in temperature. This decrease in temperature introduced an increase to the mobility due to increased lattice scattering. It is known that the formation of lattice defects (eg. dislocations) increase with decreasing deposition temperature (17). This can readily be seen in figures 9 and 10. In figure 9, the last point has a higher mobility when in fact it should have a lower mobility. And in figure 10, the second and third points behave in the same manner also due to lattice scattering.

Figure 11 illustrates the change of mobility and charge carrier concentration with temperature change.

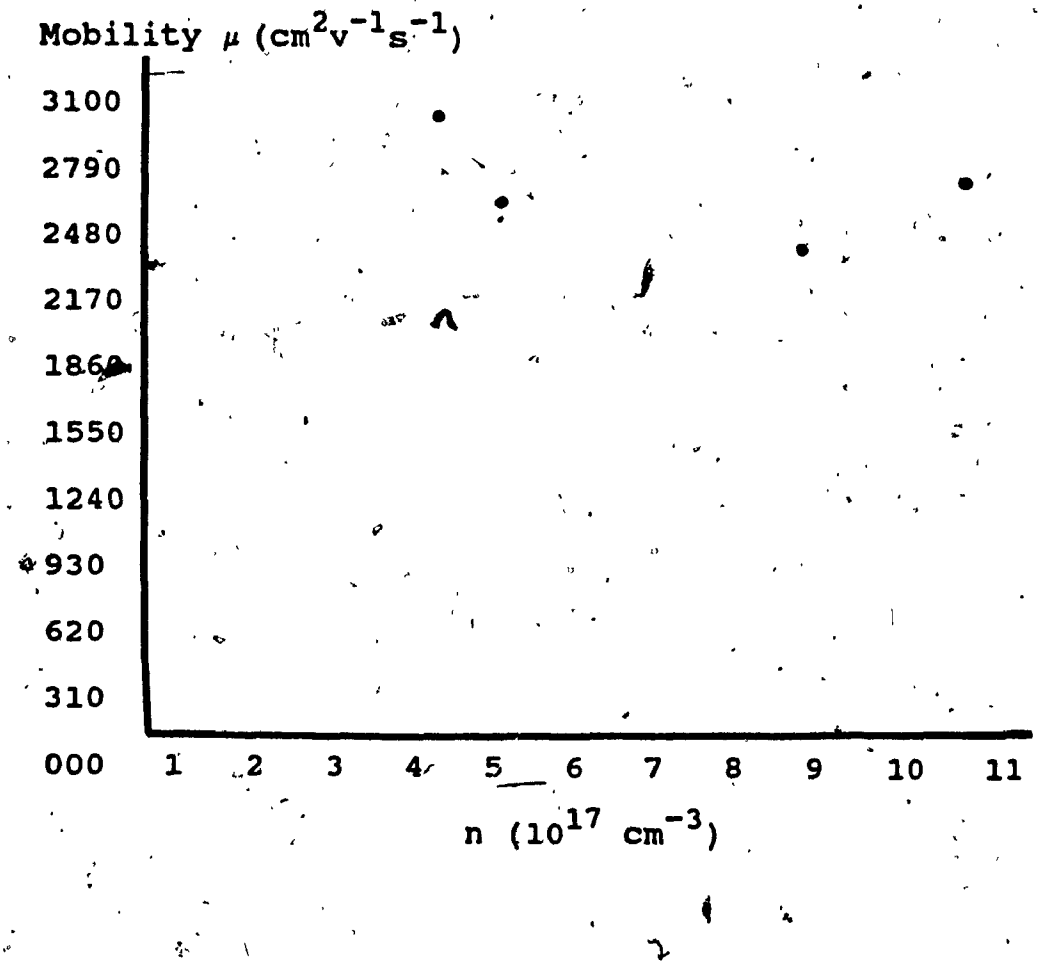

Fig. 9. Mobility variation vs charge carrier concentration (semiconductor grade graphite blocks with fused silica spacer).

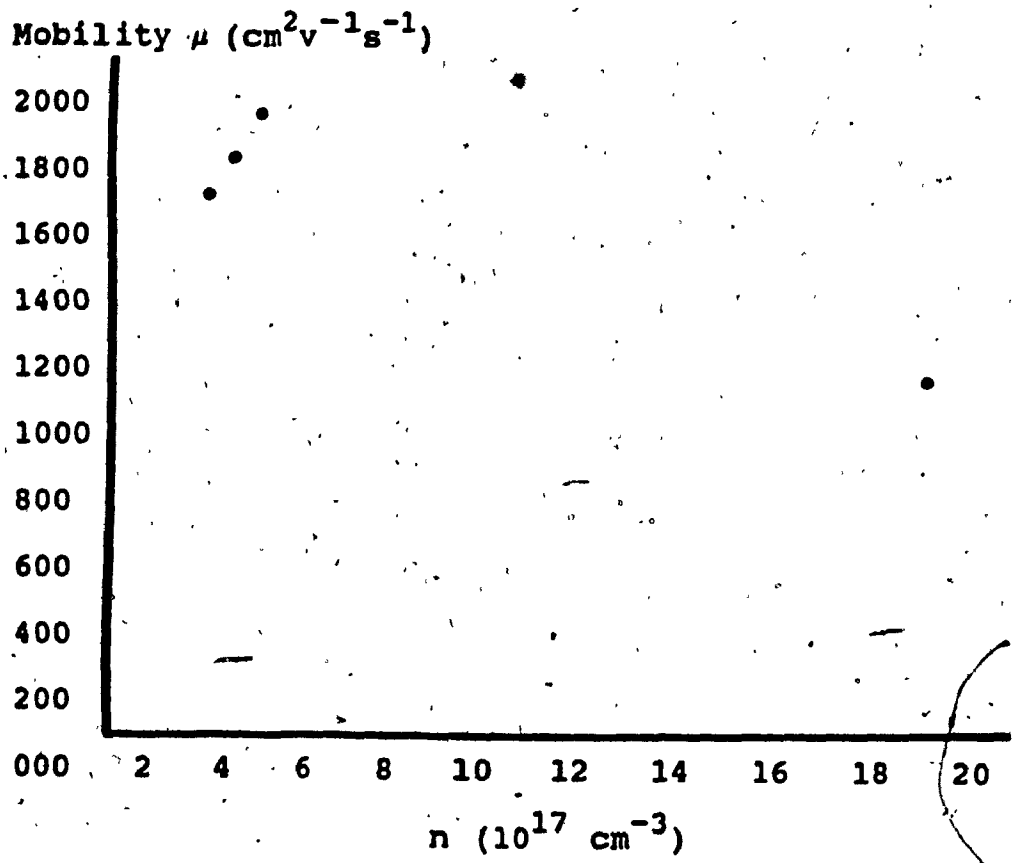

Fig. 10. Mobility variation vs charge carrier concentration (semiconductor grade graphite blocks with boron nitrite spacer).

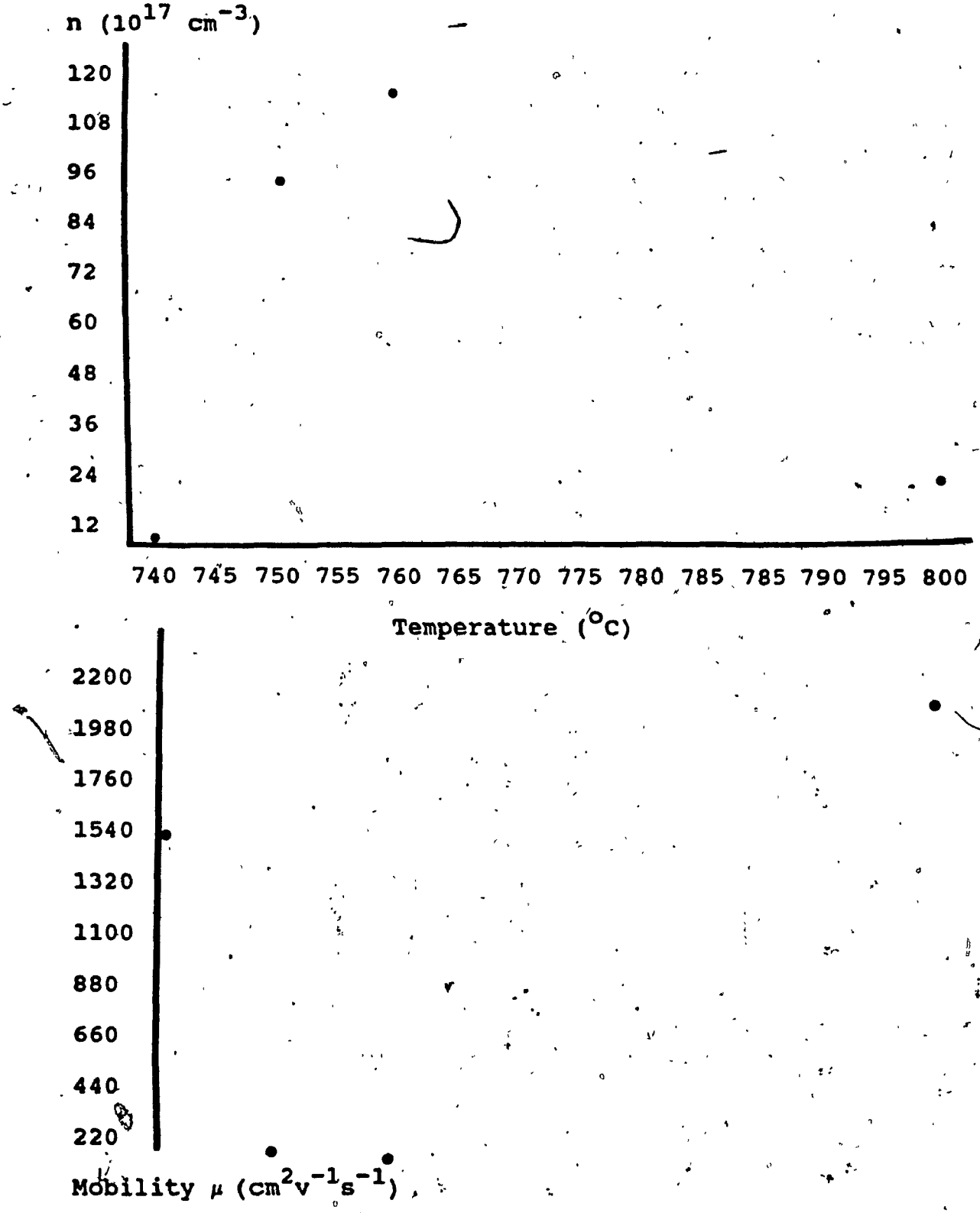

Fig. 11. Mobility variaton and charge carrier concentration vs temperature (semiconductor grade graphite blocks and spacer).

It is shown in this figure, that temperature has a great influence over mobility and concentration explaining the misplacement error. The same reasoning can be applied to figures 12, 13, and 14 which also shows the mobility versus the charge concentration for the various spacers. In general the results show an increase in mobility with a decrease in concentration. From the obtained results, most of the mobilities should have been a little higher. The highest mobility measured was of 3313 $cm^2v^{-1}s^{-1}$ for a carrier concentration of $3.9x10^{16}$ cm^{-3}. For such a concentration, a mobility of approximately 5500 $cm^{-2}v^{-1}s^{-1}$ should have been obtained (11). Misalignment on the graphite blocks is one error. Two other errors can also cause a change in results. One of these errors is predeposition, and the other is contact alignment.

Predeposition time for this system was of 12 to 15 minutes. Twelve minutes were required to obtain a source temperature of 1023 K and approximately 15 minutes were required to obtain a source temperature of 1073 K. During this interval, as the temperature was increasing, a predeposited layer was growing on the substrate. GaAs can be transported by O_2 at temperatures as low as 873 K. Since the substrate block (upper graphite block) was below the normal growth temperature, a low surface mobility epitaxial layer resulted. Hence, anything grown on this layer during deposition, will have the same structural defects, and thus a lower mobility (6).

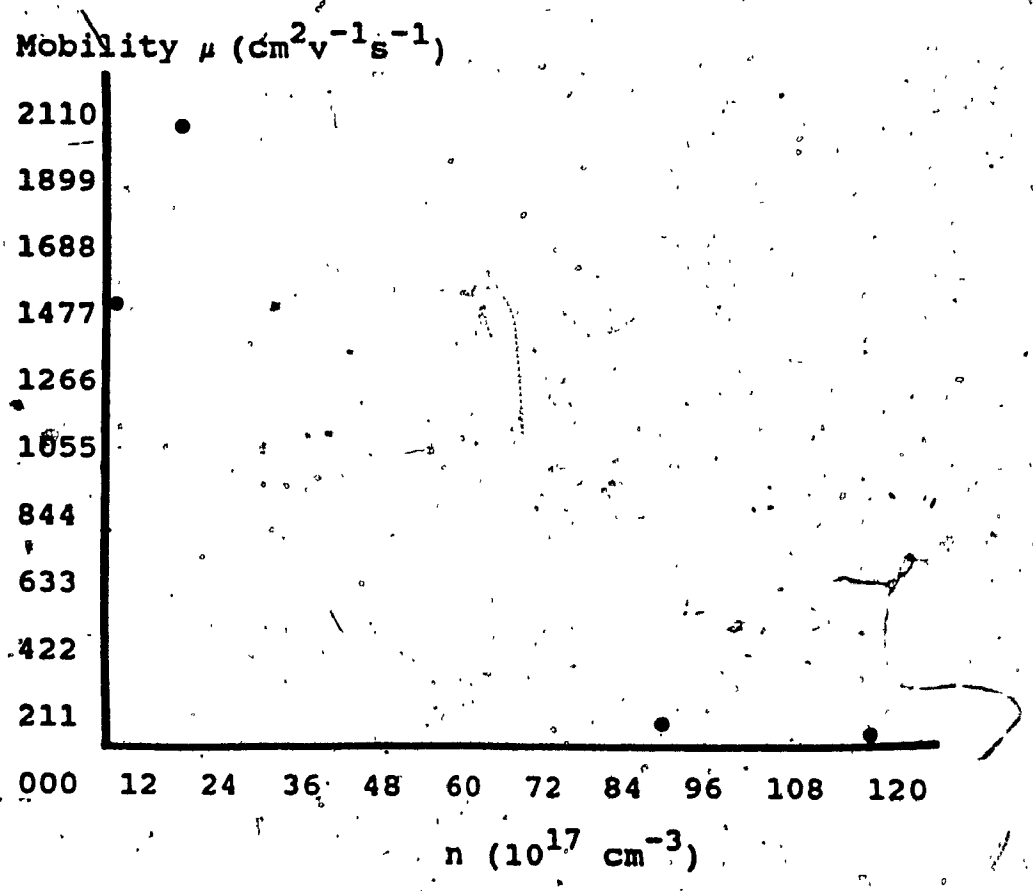

Fig. 12. Mobility variation vs charge carrier concentration (semiconductor grade graphite blocks and spacer).

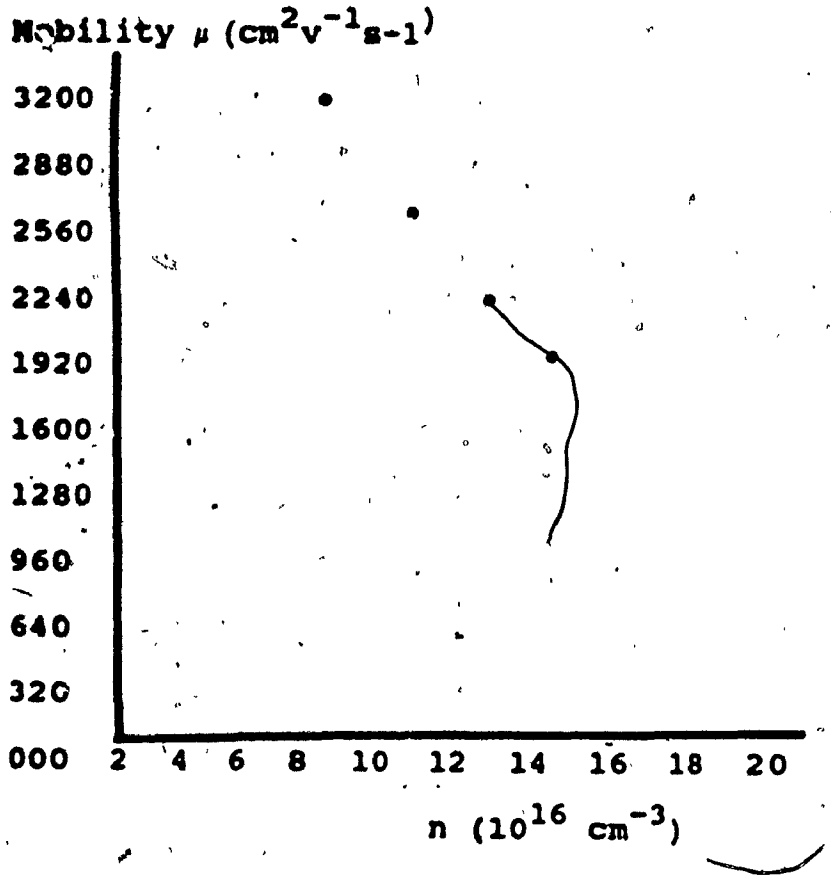

Fig. 13. Mobility variation vs charge carrier concentration (high density graphite blocks and spacer).

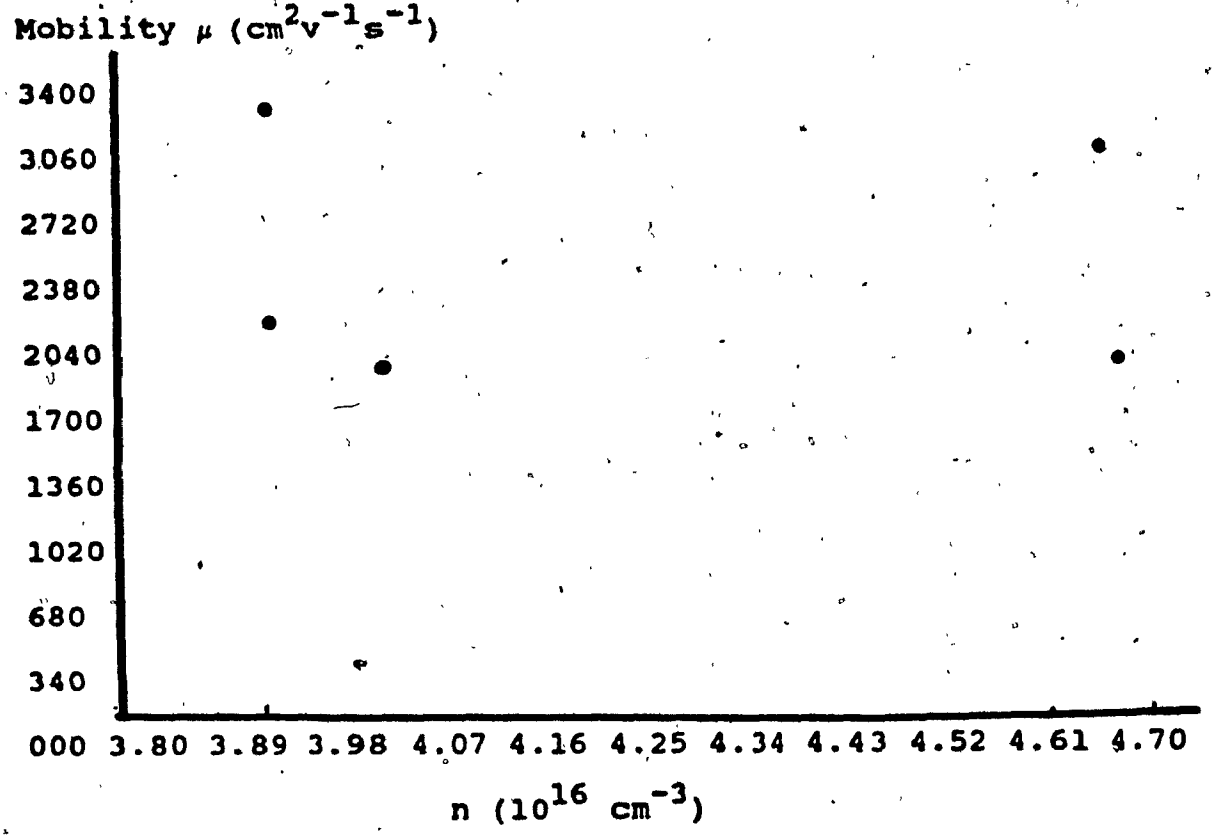

Fig. 14. Mobility variation vs charge carrier concentration (high density graphite blocks with 0.3 mm fused silica spacer).

It is therefore of great importance to reduce predeposition time to a minimum.

The other cause of error which could have slightly altered the results, is the misalignment of the contacts. When the characterization of the sample is to be done, the four contacts must be placed on the edges of the deposited layer at 90 degrees from each other. Any misplacement, either along the circumference of the deposited layer or away from the edge, will cause a percentage error thus affecting the measured results. As an example, if the measured mobility is 3313.51 $cm^2v^{-1}s^{-1}$, and a circumference error of 1.0 mm is made on all four contacts. The error percentage would be calculated as follows: (5)

$$\Delta\mu_H/\mu_H \simeq -2d/\pi^2D = -2(1.0\text{ mm})/\pi^2(6.5\text{ mm})$$
$$= -0.031 \text{ X } 4 \text{ contacts}$$
$$= -0.124,$$

where d is the misplacement error and D is the diameter of the deposited layer. Multiplying the mobility by the above result, an answer of -410.87 $cm^2v^{-1}s^{-1}$ is obtained. Therefore, the corrected mobility is of 3313.51 + 410.87 = 3724.38 $cm^2v^{-1}s^{-1}$. This misplacement of 1.0mm introduced an error of 12.4%. A similar expression can be used ($\Delta\mu_H/\mu_H = -4d/\pi^2D$) to calculate the error when the misplacement is made with respect to the edge. If both cases discussed above exist, then the errors are added to obtain the total error from both misplacements (5). Once all the percentages are added (graphite, and contact

misplacements), errors as high as 30% can be obtained. Hence, precision work is essential to lower error percentages.

4. THE EL2 COMPLEX

The EL2 antisite formation exists in an arsenic rich grown GaAs. This antisite formation has extensively been discussed in literature where gallium vacancies are at the origin of its existence (12,13).

An antisite center is formed by the occupation of a gallium vacancy by an arsenic atom of the GaAs host lattice. In a tetrahedral coordination, which is characteristic of the sp^3 hybridized molecular orbitals forming the octect of the semiconductors predominantly covalent bonds, the gallium vacancy maybe seen as being surrounded by five electrons belonging to the four neighboring arsenic atoms. The formation of an antisite complex is achieved if a neutral arsenic atom occupies the gallium vacancy. Since the arsenic atom has five valence electrons, a ten electron arrangement will result. After the completion of the octet for tetrahedral coordination, two excess electrons remain. These two electrons are assumed to be at the origin of the divalent deep lying EL2 donor centers (3). Associated to the deep lying donor level, there is a shallow monovalent donor level due to the arsenic vacancy (13). This level has a concentration equal to that of the antisite. Hence, the

EL2 complex consists of a deep lying divalent and a shallow lying monovalent donor level. The basis of this model is associated with the ratio of the measurements of the free electron concentration at room temperature and at liquid nitrogen temperature, n_{300}/n_{77} (13). The existence of the shallow donor level introduces modifications on the conditions required to achieve a high resistivity "undoped" GaAs. Deep level compensation is needed to obtain high resistivity semi-insulating material (14,15).

In an n-type material of GaAs, a deep acceptor level is required for compensation. Since the EL2 complex contains shallow donors, a deep compensating acceptor level is needed to obtain SI GaAs out of n-type GaAs (3).

4.1 Analysis of the EL2 Complex

The multilevel model based on the Shockley curves was adapted to the antisite-arsenic vacancy complex model. From this model, the determination of the degree of electron occupancy of all the impurity energy levels is obtained. The Fermi level is positioned by the neutrality condition giving the free electron and hole concentrations (7). This model has been successfully applied to analyze the occurrence of chromium doped semi-insulating GaAs (14). The maximum Ga vacancy concentration of 4×10^{18} cm^{-3} ($=N_1$) is due to a phase extent of 0.001 % in GaAs (7).

The Shockley curves are obtained by calculating the concentrations of all the ionized impurities, donors and

acceptors, and the free electron and hole concentrations, as a function of energy. The classical expressions describing these charge dependencies are required for the numerical calculations (7).

Silicon is used as a general shallow donor of variable concentration (N_{d2}). Silicon doping (voluntary or involuntary) is a frequent occurrence in the growth of GaAs crystals and these silicon atoms are suspected of forming substitutional impurity preferentially occupying gallium vacancies. The gallium vacancy concentration available for the antisite formation is $N_1 - N_{d2}$. Then the EL2 complex concentration can be given by $N_{d3} = f \times (N_1 - N_{d2})$, where f is the fraction of unfilled gallium vacancies occupied by arsenic atoms. Therefore, $N_{d3} = As_{Ga}$. As stated before, the deep divalent donor (antisite) and the shallow monovalent donor(arsenic vacancy) forming the EL2 complex, are present in equal concentrations, N_{d3}. The gallium vacancies can now be determined by $N_{a1} = N_1 - (N_{d2} + N_{d3}) = V_{Ga}$.

The Fermi level can be determined from the neutrality condition:

$$n + \Sigma(i=1 \text{ to } l)\ N_{ai}^- = p + \Sigma(j=1 \text{ to } m)\ N_{dj}^+ \quad /9/$$

where n is the density of electrons in the conduction band, p is the density of holes in the valency band, N_d^+ is the density of the holes bound to donor centers, and N_a^- is the density of electrons bound to acceptor centers. From the Maxwellian statistics, the following expressions are

used to calculate the hole concentration p, the electron concentration n, the ionized donor concentrations N_{dj}^{+}, and the ionized acceptor concentration N_{ai}^{-}:

$$p = 2(2\pi m_h kT/h^2)^{3/2} \exp(-E_f/kT) \quad /10/$$

where $m_h = 0.58\ m_o$ is the density of state effective mass of the holes, k is the Boltzmann constant, T is the absolute temperature, h is Planck's constant, and E_f is the Fermi energy.

$$N_{dj}^{+} = N_{dj}(1+g \exp(E_{dj}+E_f-E_g/kT)^{-1}$$

where g is the degeneracy factor. This factor is 2 for shallow donors and for the deep lying donors and acceptors. N_{dj} is the appropriate donor concentration, described above, corresponding to silicon, EL2 and arsenic vacancy densities. E_{dj} is their respective activation energies (3). E_g is GaAs's band gap given by:

$$E_g(T) = 1.522 - (5.8\times10^{-4}T^2/T+300) \quad (14).$$

$$n = 2(2\pi m_e kT/h^2)^{3/2} \exp(-E_g-E_f/kT)^{-1}$$

where the density of state effective mass of the electrons $m_e = 0.069\ m_o$.

Finally, $N_{ai}^{-} = N_{ai}(1+g \exp(E_{ai}-E_f/kT)^{-1}$

where N_{ai} is the deep lying compensating gallium vacancy concentration ($N_{al} = V_{Ga}$ with its activation energy E_a).

From the above expressions, the Fermi energy can be determined by calculating the charge concentrations with E_f as the running variable. The Fermi's level position is then given by the value of E_f for which the neutrality

equation, equation /9/, is satisfied. The concentrations of the free electrons, free holes, and ionized impurities can be calculated to characterize the overall transport properties of the material at this energy (3).

An EL2 concentration was assumed to be $2x10^{16}$ cm^{-3} to verify the existence of the EL2 complex, with the inclusion of the shallow donors associated to the antisites. No compensating gallium vacancies are considered (13). By adjusting the silicon concentration, the free electron concentration was varied. The mulitilevel analysis was then used to calculate the theoretical ratio of the free electron concentration at room and liquid nitrogen temperatures as a function of the room temperature concentration. From this plot, the indication of the existence of EL2 complex in an arsenic rich GaAs can be confirmed. As the concentration ratio n_{300}/n_{77} increases, a decrease of n at lower temperatures is confirmed. This freezout only occurs in samples which exhibit the EL2 complexes. An EL2-free sample would have its ratio of n_{300}/n_{77} remain very close to 1.00. It is the above result, n_{300}/n_{77}, which strengthens the theory of the one-to-one correspondence between the shallow donors and the EL2 level. Figure 15 supports the theory of the one-to-one correspondence by comparing DLTS EL2 measurements to n_{300}-n_{77} freezout calculations (13). Table III shows the experimental results of the concentration measured at 77 K and 300 K. Figure 16 illustrates the ratio of the charge

carrier concentrations n_{300}/n_{77} versus the room temperatue concentrations.

TABLE III Results obtained at 77 K and 300 K.

n_{300} (cm^{-3})	n_{77} (cm^{-3})	n_{300}/n_{77}
7.95×10^{16}	4.32×10^{16}	1.84
9.11×10^{16}	5.04×10^{16}	1.81
$7.66 \times 10_{16}$	4.36×10^{16}	1.76
4.30×10^{17}	3.67×10^{17}	1.17
4.79×10^{18}	4.80×10^{18}	1.00

As the donor doping increases, the n_{300}/n_{77} ratio decreases as shown in the above figure. Four of the samples were deposited with the high density graphite blocks and spacer while the other two were deposited with boron and fused silica spacers using the semiconductor grade blocks. The four lowest concentrations obtained from the above measurements occurred with the high density graphite. The highest concentration was obtained from the boron nitride spacer deposition.

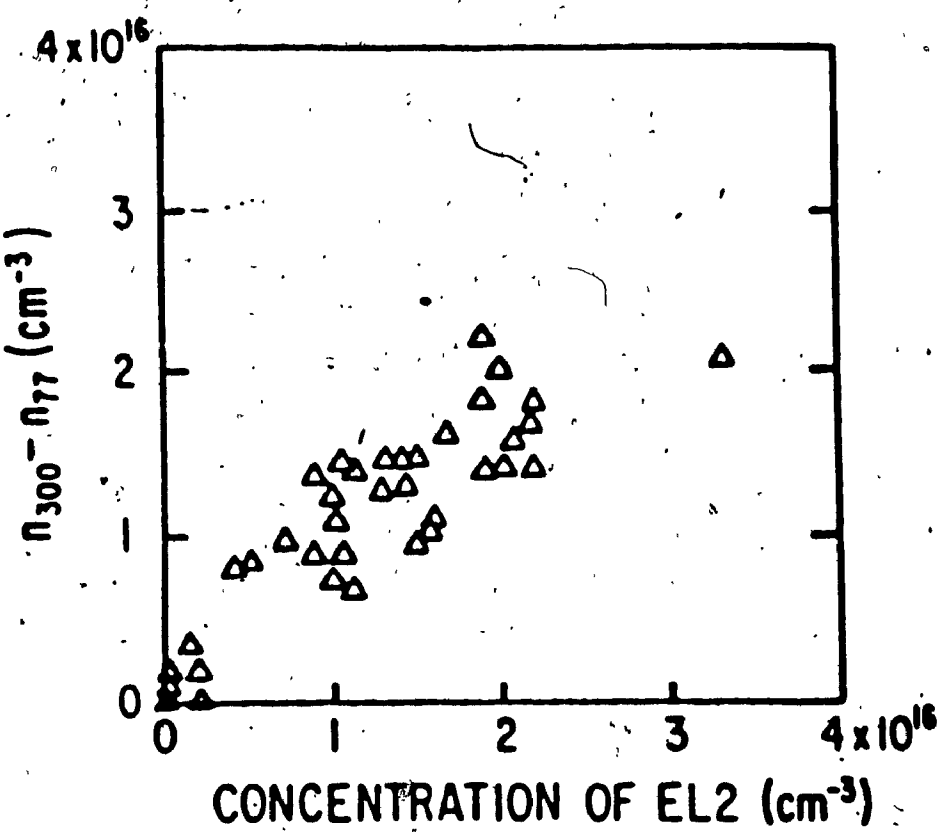

Fig. 15. $n_{300}-n_{77}$ vs EL2 concentration measurements.

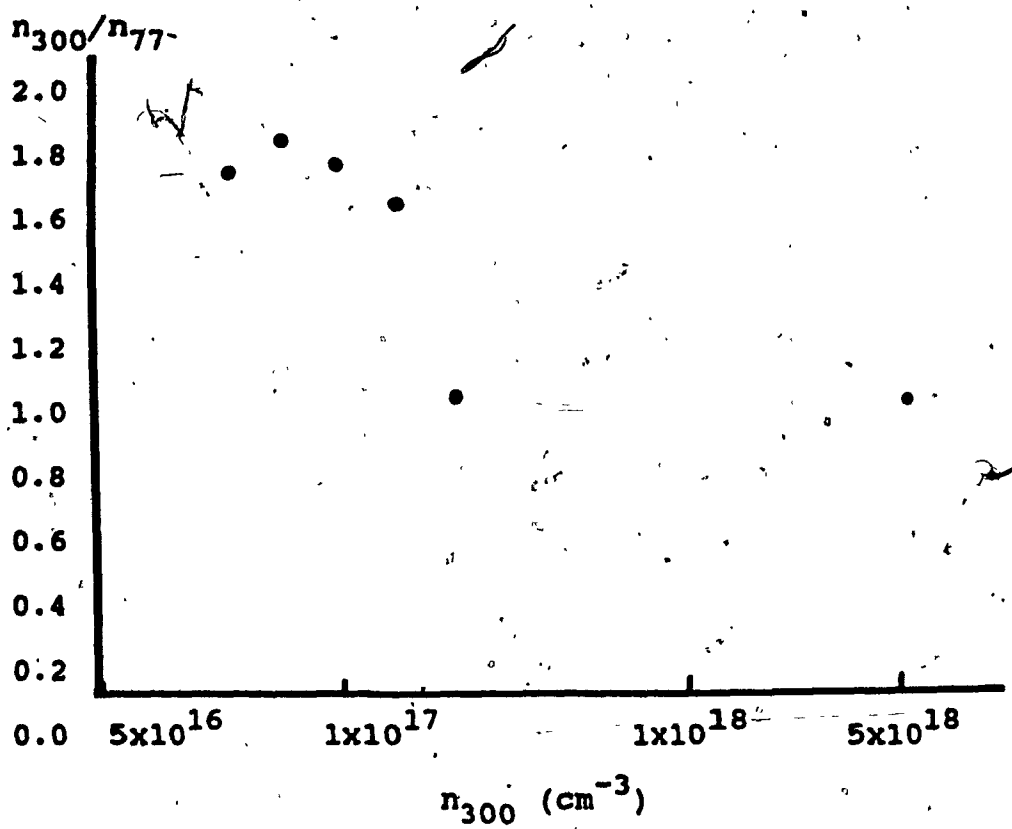

Fig. 16. n_{300}/n_{77} vs room temperature concentration (semiconductor grade graphite blocks with boron nitrite and fused silica spacers, and high density graphite blocks and spacer).

It can be seen from figure 16, that as the concentration gets very high, example the deposition with boron nitride spacer, the freezout at lower temperatures becomes annihilated. Thus, these results agree with the above discussion, and the same shallow donor levels, in the order of $1x10^{16}$ cm^{-3}, can be associated with the presence of EL2 for the CSVT GaAs system.

Figures 17, 18, and 19 were obtained from the multilevel model. The total initial gallium vacancy concentration was taken to be $N_1 = 3x10^{17}$ cm^{-3} (from the phase extent) and f = 0.15 (the fraction of arsenic which occupied gallium vacancies to form the antisite complexes). From the multilevel model, the gallium vacancy doping in the arsenic rich GaAs can be examined.

If the silicon concentration is taken to be; $N_{d2} = 2x10^{17}$ cm^{-3}, the unfilled gallium vacancy is $N_{a1} = N_1 - (N_{d2} + N_{d3})$ where,

$N_{d3} = f \times (N_1 - N_{d2})$.

Therefore,

$N_{d3} = 0.15(3x10^{17} - 2x10^{17}) = 0.15(1x10^{17}) = 1.5x10^{16}$ cm^{-3}. Knowing N_{d3}, N_{a1} can be calculated. $N_{a1} = 3x10^{17} - (2x10^{17} + 1.5x10^{16}) = 8.5x10^{16}$ cm_{-3}.

Since $N_{a1} < N_{d2}$ the material is obviously n-type with a Fermi energy of 1.39 eV and a free electron density of $7.8x10^{16}$ cm^{-3}. This is shown is figure 17.

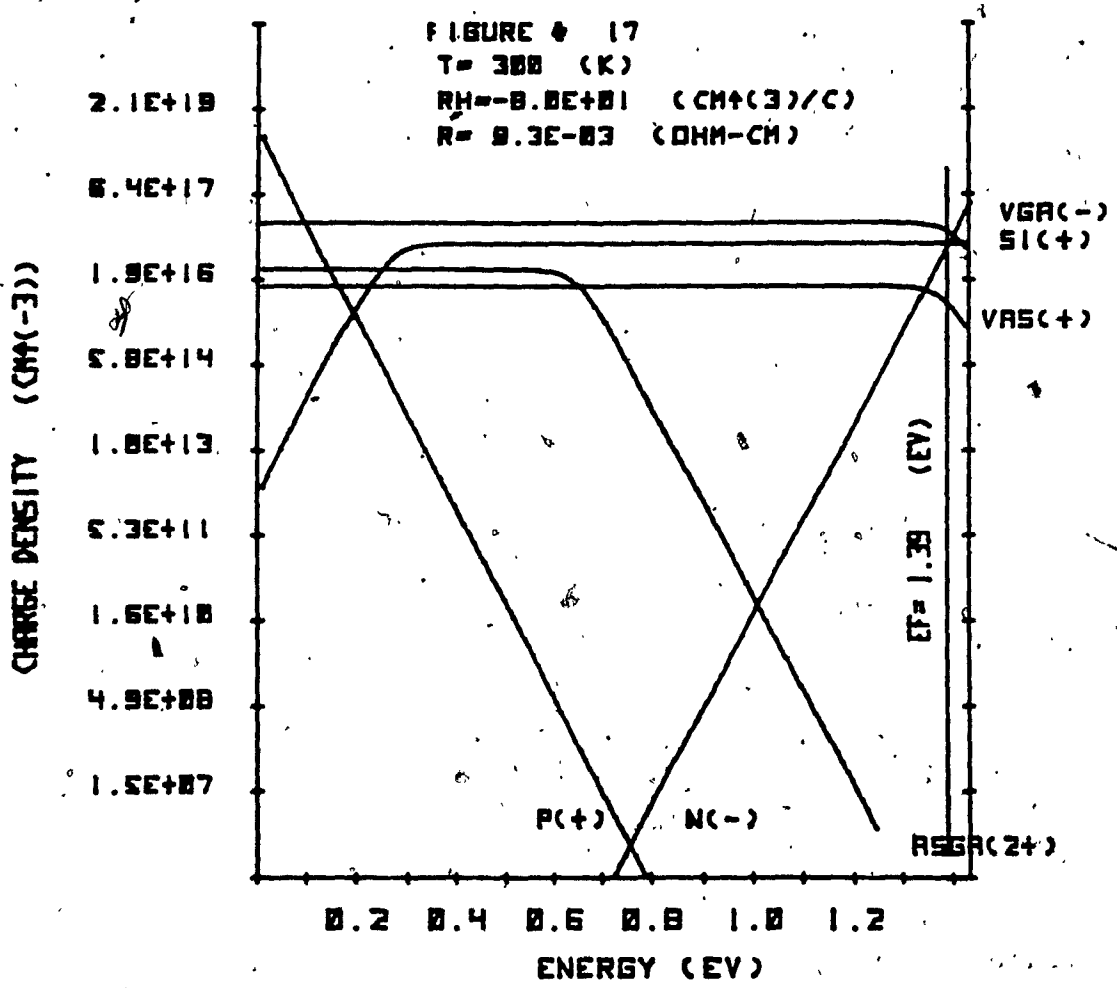

Fig. 17. Calculated charge carrier density as a function of energy to determine E_f = 1.39 eV n-type SC GaAs.

As the silicon concentration is lowered, the Fermi energy begins to decrease. The silicon concentration can be lowered by using a highly silicon doped ($1x10^{18}$ cm^{-3}) semi-conducting GaAs source for the deposition. The silicon reacts with the oxygen of the water vapor forming SiO. At deposition temperatures, SiO formations leaves the CSVT system. Thus, decreasing the shallow donor concentration in the epitaxial layer. This reduction in concentration decreases the Fermi level towards the semi-insulating range. So if the silicon concentration is decreased to $1.23x10^{17}$ cm^{-3} with all other values kept constant, the unfilled gallium vacancy increases to $1.5x10^{17}$ cm^{-3}. Hence, since the unfilled gallium vacancy concentration is greater than the sum of all other donor concentrations, the material becomes semi-insulating. The Fermi energy is located at 0.77 eV corresponding to a free electron concentration of $3x10^{6}$ cm^{-3}, and a free hole concentration of $1.1x10^{6}$ cm^{-3}. Figure 18 illustrates this case. The final case is shown in figure 19. In this case the silicon concentration is lowered to $2x10^{16}$ cm^{-3} to obtain a p-type material with a Fermi energy of 0.28 eV and a free hole concentration of $2x10^{14}$ cm^{-3}. In all figures, the ionized impurity concentrations are depicted as Si^{+} shallow donor, As_{Ga}^{2+} deep EL2 donor, V_{AS}^{+} shallow donor arsenic vacancy, and V_{GA}^{-} deep acceptor gallium vacancy (6).

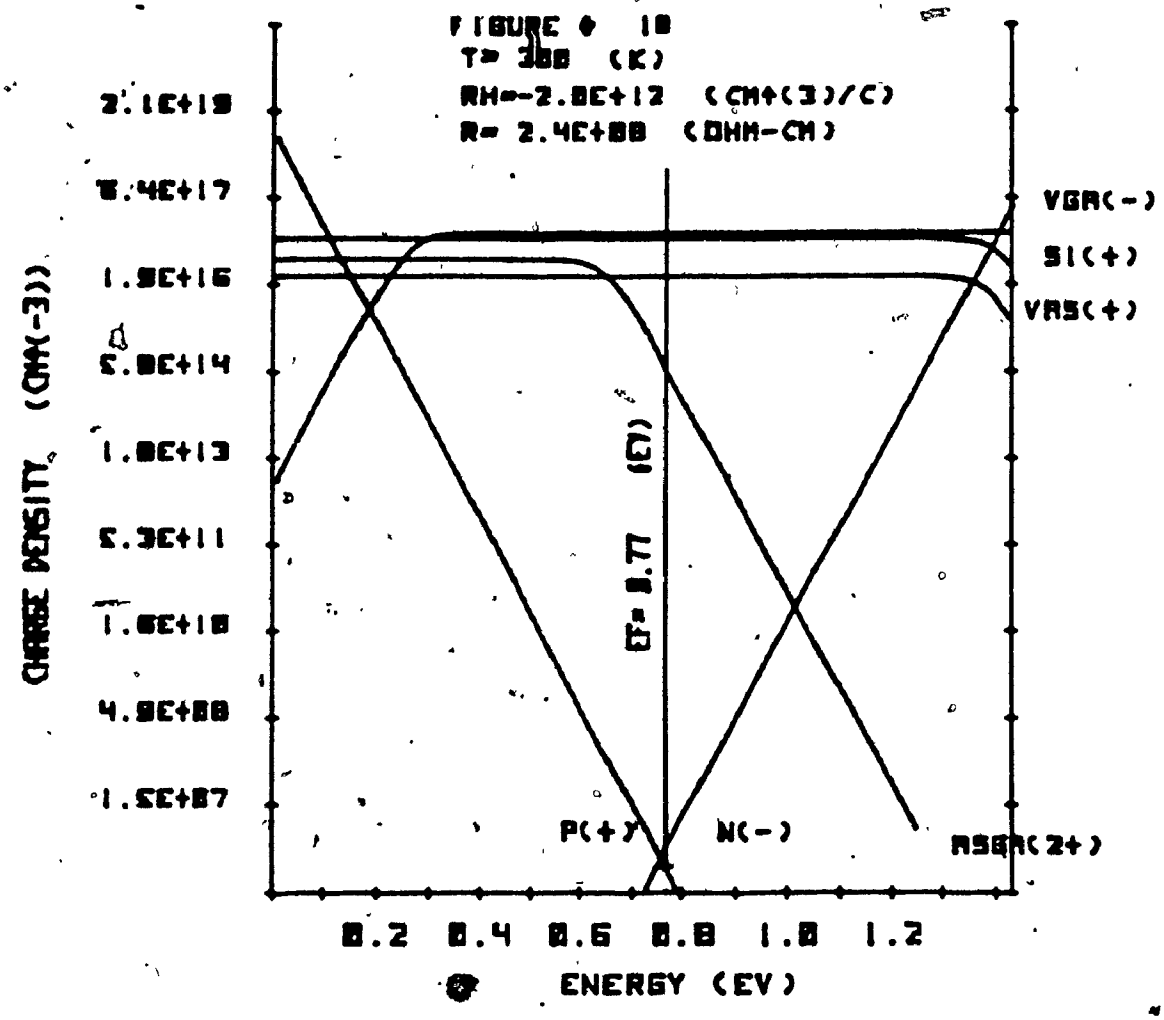

Fig. 18. Calculated shape carrier density as a function of energy to determine E_f = 0.77 eV SI GaAs.

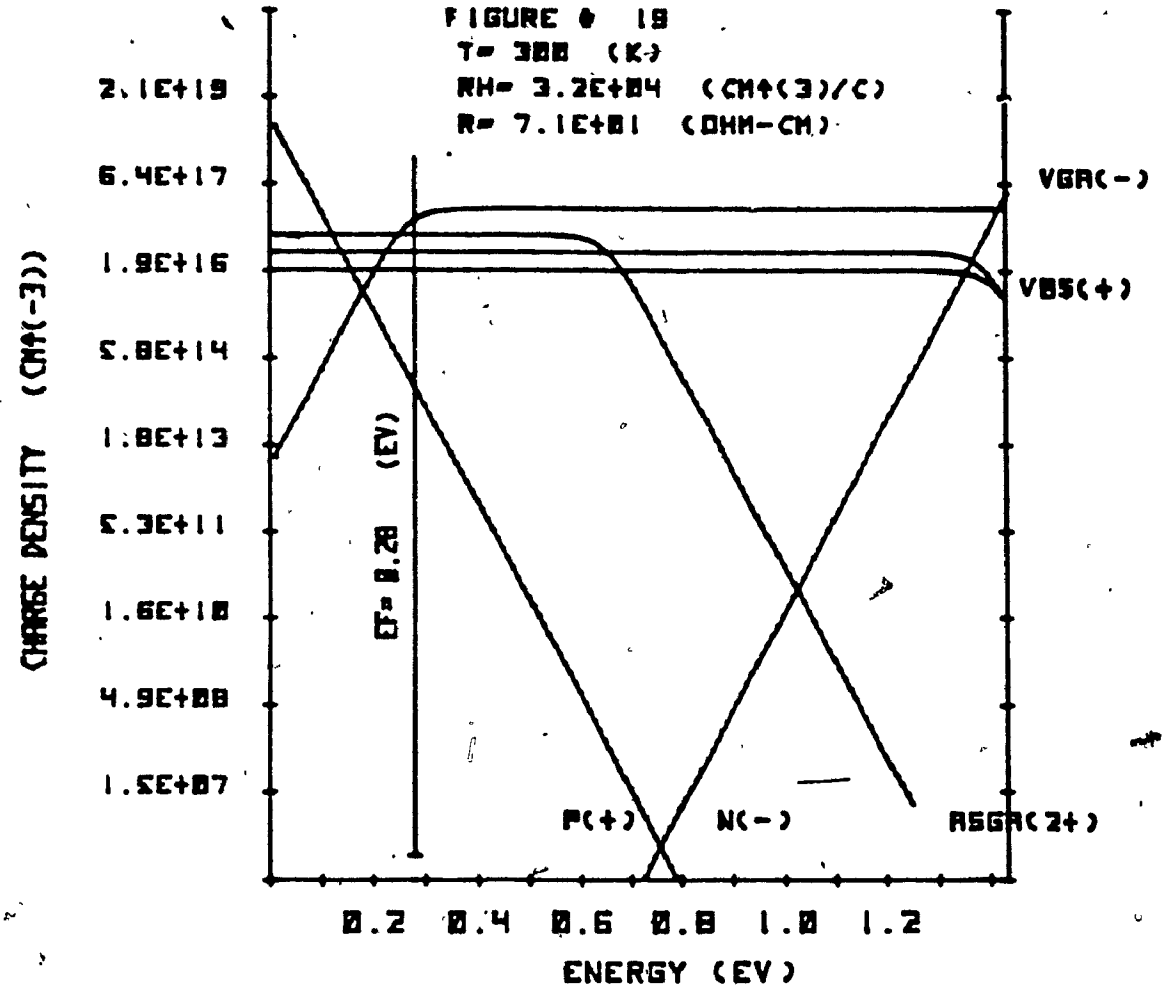

Fig. 19. Calculated charge carrier density as a function of energy to determine E_f = 0.28 eV p-type SC GaAs.

5. THE HIGH CARRIER CONCENTRATION IMPURITY

Besides the EL2 complex, another factor exists during the deposition reaction, which would explain the high concentration of $1x10^{18}$ (and higher) cm^{-3}. These donors are introduced through the graphite blocks. The shallow donors associated with GaAs are silicon, germanium, tin, selenium, sulfur, and tellurium. To exactly identify the donor is difficult. Silicon has been suggested as the major shallow dopant during the reaction (16). But what is certain, is the fact that when a low grade graphite is used the contamination is much higher. From table II, it is shown that the worst case occurred with the semiconductor grade graphite blocks and spacer. Because of its high porous character, the highest concentration level obtained was $1.15x10^{19}$ cm^{-3}. When a high density graphite block and spacer was used, the concentration lowered by a factor of ten. The worst case being $1.61x10^{17}$ cm^{-3}. Also from table II, it is easily observed that the only time a concentration higher than $1x10^{18}$ cm^{-3} is obtained is when the semiconductor grade graphite blocks are in use. The greatest factor difference found between the semiconductor (using a graphite spacer) and the high density graphite blocks (using a fused silica spacer) was of 20. In both cases, the factor difference between the fused silica and graphite spacers was of 1.68, for the semiconductor grade graphite, and of 1.96 for the high density grade

graphite. The doping impurities can be reduced by using very high density graphite blocks.

6. GaAs SOLAR CELLS

Semi-conducting (SC) and semi-insulating GaAs have both been successfully deposited on germanium (Ge). The use of germanium as a substrate for GaAs solar cells has many advantages. The germanium substrate is 20 to 50% lower in cost and has a thermal conductivity of 50% higher than GaAs substrates. The Ge/GaAs heteroepitaxial structure is made possible since both have very similar lattice constants. Solar cell fabrication using GaAs and Ge can be implemented by using the closed spaced vapor transport (CSVT) system.

The orientation of the Ge substrates can be in the <100> or <111> direction. These crystals would be grown using the Czochralski crystal grower. The CSVT system would be used to deposit four layers to form the solar cell. First, a p^+ Ge substrate with an acceptor concentration of $8x10^{18}$ cm^{-3} would be used as the substrate of the solar cell. The high concentration of the Ge substrate would be necessary so that during the deposition the arsenic (As) concentration would be less than that of the germanium. The second layer of the solar cell would be a GaAs p^+ buffer layer. This layer would be highly doped with zinc (Zn) and its main function would consist of over doping any Ge diffusing into the GaAs during the epitaxial growth. The

hole concentration of $5x10^{18}$ cm^{-3} in the buffer layer would have to be decreased to $1x10^{17}$ cm^{-3} in the active layer so that a back-surface field is obtained providing an increase in the collection efficiency. The final layer of the solar cell would be a GaAs n^+ with a concentration of $5x10^{18}$ cm^{-3}. Figure 20 illustrates the solar cell. The antireflection coating (AR) would have a thickness of $\lambda/4$ where λ (600nm) is the wavelength of the sun's radiation at its maximum intensity. Thus from the above calculation, the required thickness for an optimum AR coating would be 150nm. The gold (Au) and tin (Sn) contacts would be electroplated. The advantage of the Sn over the Au contacts on the n^+ GaAs layer is that with the Sn contacts, an optimization of the n^+ layer can be achieved. The anodic oxide formed on the n^+ layer can be stripped away by using a diluted HCl solution. This solution would not affect the Sn contacts. Therefore, the n^+ layer thickness can be adjusted for maximum power conversion efficiency, and then the oxide layer can be reanodized.

The typical characteristics of such a device would be as follows:

Fill Factor.....0.82

Open Circuit Voltage.....0.97 V

AM1 Efficiency.....17 to 20% (4).

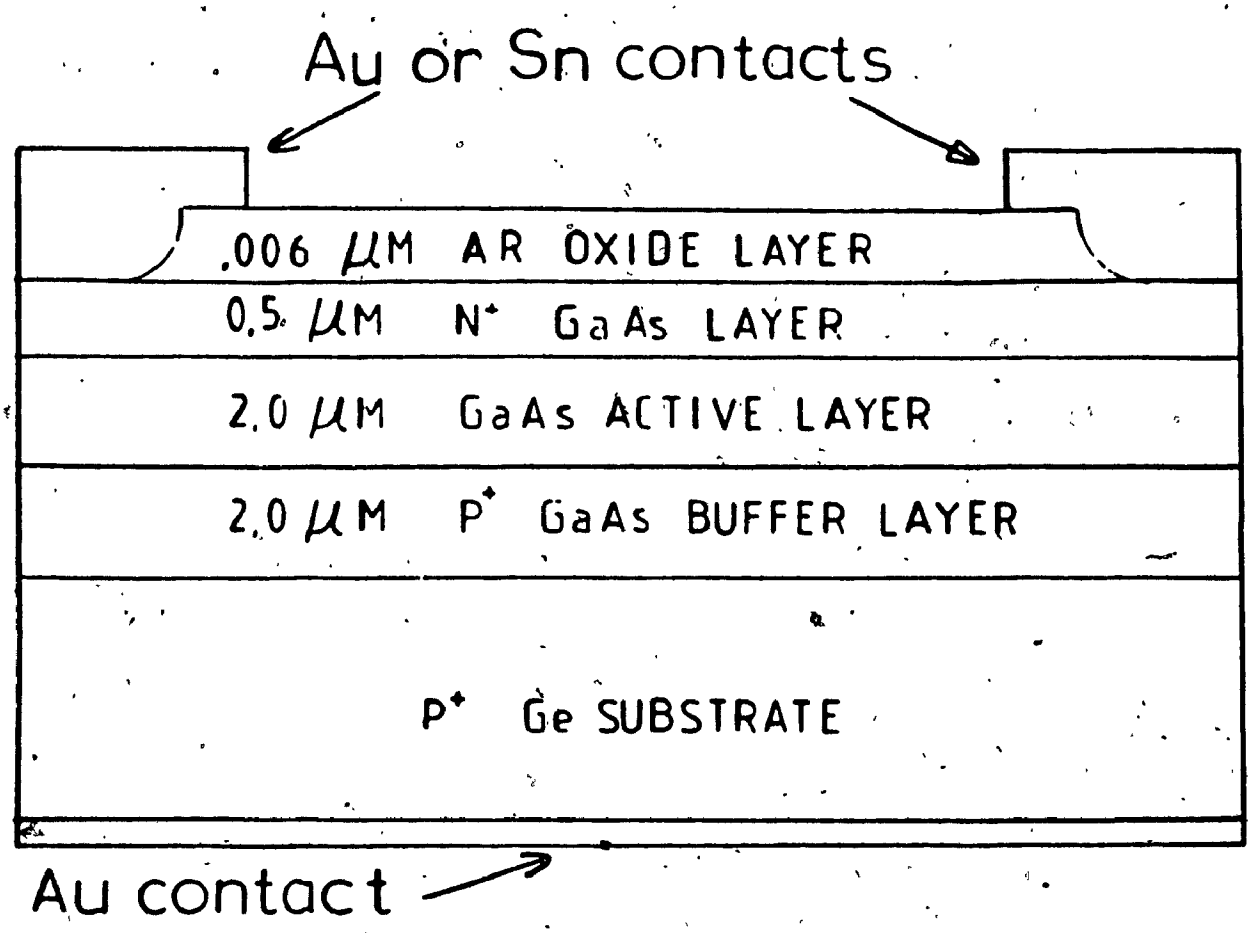

Fig. 20. Schematic representation of $n^+/p/p^+$ GaAs/Ge solar cell.

7. CONCLUSION

Epitaxial thin film gallium arsenide layers have been deposited using the CSVT system. The analysis showed that temperature was the only thermodynamical influence of the reaction. Carrier concentrations as low as 3.9×10^{16} cm^{-3} and mobilities as high as 3313 $cm^{-2}v^{-1}s^{-1}$ were measured. The equivalent thermal resistance circuit calculation showed that a surface temperature of approximately 25 K existed when using a fused silica spacer of 0.3 mm in thickness. The existence of "undoped" semi-insulating gallium arsenide was attributed to the EL2 complex which was analysed by the use of the multilevel energy model. The high concentrations in the deposited layers were directly related to the grade of the graphite which acts as an incubator for different impurities. A schematic design of a GaAs/Ge solar cell was introduced. The power conversion efficiency of this solar cell would be 17 to 20 %.

REFERENCES

1. Lombos, B.A., Dodelet, J.P., Coté, D., Dickson, I., "Epitaxy of GaAs by the Close-Spaced Vapor Transport Techinique," Journal of the Electrochemical Society , Vol. 133, No. 9, Sept. 1986, pp. 1925-1934.

2. Nicoll, F.H., "The use of close spacing in chemical transport systems for growing epitaxial layers of semiconductors," Journal of the Electrochemical Society , Vol. 110, No. 11, Nov. 1963, pp. 1165-1169.

3. Lombos, B.A., Lawrence, M., Dodelet, J.P., D'Asti, G., "Heteroepitaxial GaAs for Integrated Circuits," IEEE Montech'86 Conference , Sept. 1986, pp. 50-53.

4. Lombos, B.A., et al., "Development of Efficient Cost Effective GaAs on Ge Solar Cells," July 1985, pp. 1-4.

5. Van der Pauw, L.J., "A Method of Measuring Specific Resistivity and Hall-Effect of Discs of Arbitrary Shapes," Phillips Research Report , Vol. 13, No. 1, Feb. 1958, pp. 1-9.

6. Gottlieb, G., and J.F. Corboy, "Epitaxial Growth of GaAs Using Water Vapor," RCA Review , Vol. 24, No. 4, Dec. 1963, pp. 585-595.

7. Lombos, B.A., Dodelet, J.P., Coté, D., Dickson, I., "Thermodynamic Equilibrium Displacement Controlled Epitaxial Growth of GaAs," Journal of Crystal Growth , 1986, pp. 455-462.

8. Touloukian, Y.S., Powell, R.W., Ho, C.Y., Klemens, P.G., Thermal Conductivity, Non Metallic Solids , 1st ed., (New York: IFI/Plenum, 1970), p. 174.

9. Weast, R.C., Handbook of Chemistry and Physics , 61th ed., (Boca Raton: CRC Press, 1981) p. E-398.

10. Touloukian, Y.S., Liley, P.E., Saxena, S.C., Non Metallic Liquids and Gases , 1st ed., (New York: IFI/Plenum, 1970), p. 41.

11. Sze, S.M., Physics of Semiconductor Devices , 2nd ed., (New York: John Wiley & Sons, 1981), p. 29.

12. Lagowski, J.,et.al , "Origin of the 0.82 eV electron trap in GaAs and its annihilation by shallow donors," Applied Physics Letters , 40, Feb. 1982, pp. 342-344.

13. Walukiewicz, W., Lagowski, L., Gatos, H.C., "Shallow donor associated with the main electron trap (EL2) in melt-grown GaAs," Applied Physics Letters , 43, July 1983, pp. 112-114.

14. Lombos, B.A., N. Yemenidjian, and M. Averous, "Compensation by deep levels in semi-insulating GaAs," Canadian Journal of Physics , Vol. 60, No. 1, 1982, pp. 35-40.

15. Lombos, B.A., "Deep Levels in Semiconductors," Canadian Journal of Chemistry , Vol. 63, No. 7, 1985, pp. 1666-1671.

16. Mimila-Arroyo, J., Legros, R., Bourgoin, J.C., Chavez, F., "Photoluminescence and electrical properties of close space vapor transport GaAs epitaxial layers," The Journal of Applied Physics , Vol. 58, No. 9, Nov. 1st, 1985, pp. 3652-3654.

17. Streetman, Ben G., Solid State Electronic Devices, 2nd ed., (New Jersey: Prentice Hall, Inc., 1980), p. 85.